Article

Hyperactivation of TORC1 Drives Resistance to the Pan-HER Tyrosine Kinase Inhibitor Neratinib in *HER2*-Mutant Cancers

Graphical Abstract
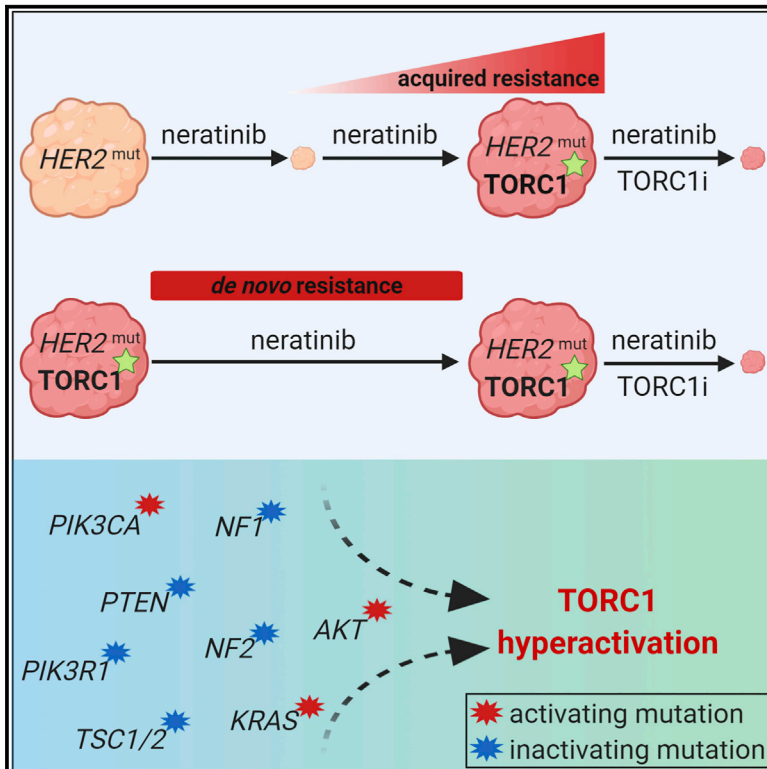
Authors

Dhivya R. Sudhan,
Angel Guerrero-Zotano, Helen Won, ...,
Alan Auerbach, Ariella B. Hanker,
Carlos L. Arteaga

Correspondence

ariella.hanker@utsouthwestern.edu
(A.B.H.),
carlos.arteaga@
utsouthwestern.edu (C.L.A.)

In Brief

In brief, Sudhan et al. identify that hyperactivation of TORC1 restores HER2 downstream signaling to drive neratinib resistance across histologically distinct *HER2*-mutant cancers. The combination of TORC1 inhibitor everolimus and neratinib arrests the growth of neratinib-resistant cells, organoids, and xenografts.

Highlights

- Neratinib resistance in *HER2*-mutant cancers is associated with TORC1 hyperactivation

- Multiple mechanisms converge on TORC1 signaling to promote neratinib resistance

- Combination with TORC1 inhibitor everolimus restores sensitivity to neratinib

CellPress

Hyperactivation of TORC1 Drives Resistance to the Pan-HER Tyrosine Kinase Inhibitor Neratinib in *HER2*-Mutant Cancers

Dhivya R. Sudhan,[1] Angel Guerrero-Zotano,[2] Helen Won,[3] Paula González Ericsson,[4] Alberto Servetto,[1] Mariela Huerta-Rosario,[1] Dan Ye,[1] Kyung-min Lee,[1] Luigi Formisano,[2] Yan Guo,[5] Qi Liu,[6] Lisa N. Kinch,[7] Monica Red Brewer,[2] Teresa Dugger,[2] James Koch,[2] Michael J. Wick,[8] Richard E. Cutler, Jr.,[9] Alshad S. Lalani,[9] Richard Bryce,[9] Alan Auerbach,[9] Ariella B. Hanker,[1,10,*] and Carlos L. Arteaga[1,10,11,*]

[1]Simmons Comprehensive Cancer Center, University of Texas Southwestern Medical Center, Dallas, TX, USA
[2]Department of Medicine, Vanderbilt University Medical Center, Nashville, TN, USA
[3]Memorial Sloan Kettering Cancer Center, New York, NY, USA
[4]Breast Cancer Program, Vanderbilt-Ingram Cancer Center, Nashville, TN, USA
[5]Comprehensive Cancer Center, University of New Mexico, Albuquerque, NM, USA
[6]Center for Quantitative Sciences, Vanderbilt University Medical Center, Nashville, TN, USA
[7]Howard Hughes Medical Institute, University of Texas Southwestern Medical Center, Dallas, TX, USA
[8]START, 4383 Medical Drive, San Antonio, TX, USA
[9]Puma Biotechnology, Inc., Los Angeles, CA, USA
[10]Department of Internal Medicine, University of Texas Southwestern Medical Center, Dallas, TX, USA
[11]Lead Contact
*Correspondence: ariella.hanker@utsouthwestern.edu (A.B.H.), carlos.arteaga@utsouthwestern.edu (C.L.A.)
https://doi.org/10.1016/j.ccell.2019.12.013

SUMMARY

We developed neratinib-resistant *HER2*-mutant cancer cells by gradual dose escalation. RNA sequencing identified TORC1 signaling as an actionable mechanism of drug resistance. Primary and acquired neratinib resistance in *HER2*-mutant breast cancer patient-derived xenografts (PDXs) was also associated with TORC1 hyperactivity. Genetic suppression of RAPTOR or RHEB ablated P-S6 and restored sensitivity to the tyrosine kinase inhibitor. The combination of the TORC1 inhibitor everolimus and neratinib potently arrested the growth of neratinib-resistant xenografts and organoids established from neratinib-resistant PDXs. RNA and whole-exome sequencing revealed RAS-mediated TORC1 activation in a subset of neratinib-resistant models. DNA sequencing of *HER2*-mutant tumors clinically refractory to neratinib, as well as circulating tumor DNA profiling of patients who progressed on neratinib, showed enrichment of genomic alterations that converge to activate the mTOR pathway.

INTRODUCTION

Large-scale tumor genome profiling efforts such as The Cancer Genome Atlas (TCGA) have identified recurrent somatic mutations in the human epidermal growth factor receptor 2 (*HER2/ERBB2*) gene, many of which have been pre-clinically and clinically proven to be oncogenic drivers (Bose et al., 2013; Hyman et al., 2018; Kavuri et al., 2015; Zabransky et al., 2015). Somatic

HER2 mutations mostly occur in the absence of gene amplification and have been noted across breast (∼3%), cervical (∼4%), lung (∼3%), colorectal (∼4%), and bladder cancers (∼9%) (cBioPortal.org). The prevalence of *HER2* mutations is even higher in metastatic breast cancers progressing after primary endocrine therapy (∼6%) and has been causally associated with anti-estrogen resistance (Croessmann et al., 2019; Nayar et al., 2019; Razavi et al., 2018). Mutations in the HER2

Significance

The HER2 tyrosine kinase inhibitor neratinib is clinically active in patients with *HER2*-mutant cancers. However, responses are heterogeneous across tumor types and generally short lived, suggesting mechanisms of *de novo* and acquired resistance. We found that TORC1 hyperactivation, leading to restoration of the signaling axis downstream of HER2, drives neratinib resistance across histologically distinct *HER2*-mutant cancers. Interrogation of genomic data from *HER2*-mutant cancers that were treated with neratinib revealed the presence of mTOR pathway-activating alterations in patients exhibiting *de novo* or acquired resistance to neratinib. Thus, we propose that the combination of neratinib with TORC1 inhibitors is worthy of clinical investigation in *HER2*-mutant cancers harboring concurrent alterations that activate the mTOR pathway.
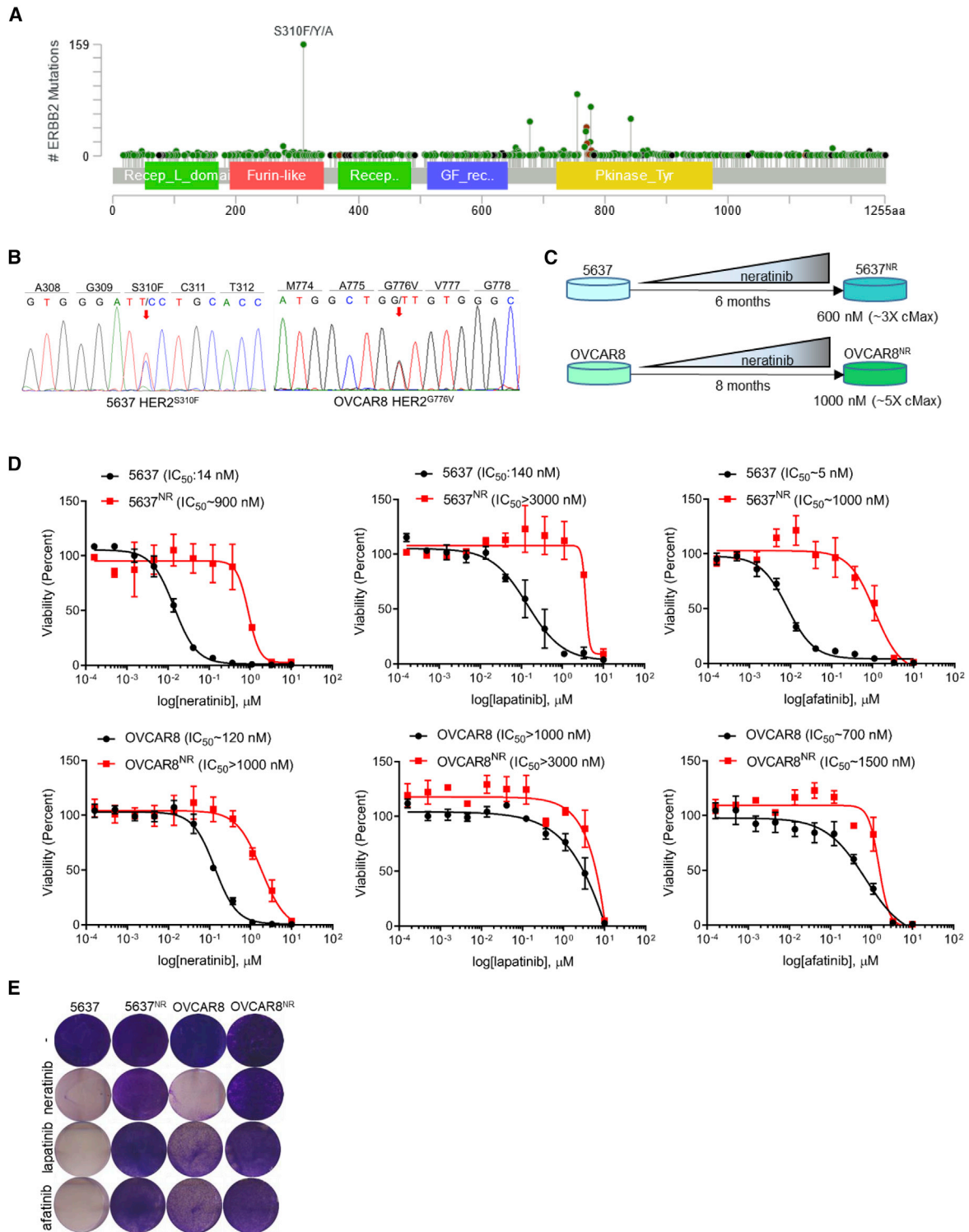
Figure 1. Generation and Characterization of *HER2*-Mutant Cells with Acquired Resistance to Neratinib

(A) Lollipop plot showing prevalence of different *HER2* mutations in 1,488 samples queried across 53,929 tumors (cBioPortal).

(B) Electropherograms of *HER2* cDNA depicting gain-of-function mutations in 5637 and OVCAR8 cells.

(C) Schematic representation of generation of neratinib-resistant 5637 and OVCAR8 cell lines. cMax, maximum plasma concentration.

extracellular and kinase domains have been shown to constitutively activate the receptor's tyrosine kinase activity and downstream phosphatidylinositol 3-kinase (PI3K) and mitogen-activated protein kinase (MAPK) signaling (Croessmann et al., 2019; Zabransky et al., 2015).

The irreversible pan-HER tyrosine kinase inhibitor (TKI) neratinib has demonstrated significant anti-tumor activity in pre-clinical models of breast, colorectal, and non-small cell lung cancer with *HER2* mutations (Bose et al., 2013; Kavuri et al., 2015; Shimamura et al., 2006). Encouraged by these promising results, phase II trials such as the MutHER trial in metastatic breast cancer and the SUMMIT basket trial explored the clinical efficacy of neratinib in patients with *HER2*-mutant cancers (Hyman et al., 2018; Ma et al., 2017). Recently published results from the SUMMIT trial demonstrate clinical benefit from neratinib in patients with breast, cervical, and biliary cancers. However, neratinib was ineffective against colorectal, gastroesophageal, and ovarian cancers harboring *HER2* missense mutations. These disparities in clinical benefit suggest the presence of genomic modifiers of response and, in turn, the need to develop rational drug combinations to circumvent *de novo* drug resistance. Further, even those patients deriving benefit from neratinib eventually progress with drug-resistant metastatic disease. In this study, we aimed to identify clinically actionable mechanisms of resistance to neratinib in *HER2*-mutant cancers and provide a therapeutic strategy to restore response in tumors exhibiting primary or acquired resistance to neratinib.

RESULTS

Neratinib-Resistant *HER2*-Mutant Cancer Cells Are Cross-resistant to Other HER2 TKIs

Although gain-of-function mutations in *HER2* occur throughout the length of the gene, extracellular domain S310F/Y/A mutations and kinase domain mutations are most prevalent (Figure 1A). We therefore chose 5637 bladder cancer cells with *HER2*^{S310F} and OVCAR8 ovarian cancer cells with *HER2*^{G776V} kinase domain mutations to model neratinib resistance (Figures 1B and S1A–S1C). Drug-resistant 5637 and OVCAR8 cells (hereafter referred to as 5637^{NR} and OVCAR8^{NR}, respectively) were generated by gradually exposing neratinib-sensitive parental cells to increasing concentrations of the drug until resistance was achieved (Figure 1C). 5637^{NR} and OVCAR8^{NR} cells grew exponentially at concentrations that were ~3× (600 nM) and ~5× (1 μM) higher than the maximum plasma concentration of neratinib achieved in patients (Wong et al., 2009). Systematic 12-point dose-response assessments of 5637^{NR} and OVCAR8^{NR} cells treated with neratinib showed an ~50- and 10-fold shift in IC$_{50}$ values compared with drug-sensitive parental cells (Figures 1D and 1E). We next tested the sensitivity of 5637^{NR} and OVCAR8^{NR} cells to other FDA-approved HER2 TKIs such as lapatinib and afatinib. Whereas parental 5637 cells

were sensitive to these drugs, 5637^{NR} cells were highly resistant to both lapatinib and afatinib as indicated by a 20- and ~200-fold increase in their IC$_{50}$, respectively. OVCAR8 cells, on the other hand, showed intrinsic resistance to lapatinib; OVCAR8^{NR} cells were highly resistant to both TKIs. To test the stability of neratinib resistance, 5637^{NR} and OVCAR8^{NR} cells were either cultured continually in the presence of neratinib or maintained under drug-free conditions (Figures S1D and S1E). Neratinib sensitivity of drug-free cells was compared with that of cells continually maintained in the presence of the drug. The 5637^{NR} and OVCAR8^{NR} cells retained their drug-resistant phenotype even after prolonged neratinib withdrawal, suggesting that the cells may have acquired a stable mechanism of drug resistance.

The TORC1 Pathway Is Hyperactivated in Neratinib-Resistant Mutant-*HER2* Cells

In order to identify mechanisms of resistance to neratinib, we first performed RNA sequencing (RNA-seq). We posited that an in-depth comparison of the transcriptome of sensitive versus resistant cells, both in the presence of the TKI, would precisely highlight transcriptional programs that are responsive to neratinib in sensitive cells but remain recalcitrant to treatment in a resistant population (Figure 2A). This approach might closely recapitulate transcriptomic differences in tumors at the time of clinical response versus progression. This approach also filters out any early responses triggered by acute drug exposure that may not be related to drug resistance. We noted a striking difference in gene expression profiles of parental and neratinib-resistant cells (Figures S2A and S2B). Gene set enrichment analysis of neratinib-resistant cells showed enrichment of cell-cycle-promoting E2F targets compared with parental cells, suggesting that 5637^{NR} and OVCAR8^{NR} cells had retained their resistant phenotype after the week-long drug washout (Figure 2B). In addition, we observed enrichment of other gene sets including NF-κB, epithelial-to-mesenchymal transition (EMT), KRAS, TORC1, inflammation, and immunological signatures.

HER2-activating mutations occur across a wide spectrum of tumor types, and HER2 TKIs, like neratinib, are clinically active against a significant fraction of these cancers (Hyman et al., 2018). Therefore, to capture actionable targets that would apply to a wide range of *HER2*-mutant tumor types, we generated a resistance-associated expression signature by identifying genes that were commonly perturbed in both neratinib-resistant cell lines (Figure 2A), and performed connectivity map analysis of the top 150 upregulated and downregulated genes in this overlap list (Figure 2C). This analysis generates a list of drugs that are rank ordered by median score based on their effect on 9 cancer cell lines (Subramanian et al., 2017). A negative median score indicates that the corresponding drug would elicit a gene expression pattern opposite to the query signature. Several inhibitors of the mTOR and PI3K pathways topped the list of drugs that could reverse the gene signature associated with neratinib resistance.

(D) Twelve-point dose-response curves of parental and neratinib-resistant 5637 and OVCAR8 cells treated with neratinib, lapatinib, or afatinib. After 6 days of treatment, cells were counted on a Coulter counter. Each data point represents the percentage cell viability relative to vehicle-treated controls. Shown are the mean viability ± SEM from at least two independent experiments.

(E) Images of crystal violet-stained monolayers of parental and neratinib-resistant 5637 and OVCAR8 cells seeded in 12-well plates and treated with HER2 TKIs (1 μM).

See also Figure S1.

Figure 2. The TORC1 Pathway Is Hyperactivated in Neratinib-Resistant *HER2*-Mutant Cells

(A) Schema of RNA-seq analysis of parental and neratinib-resistant 5637 and OVCAR8 cells. DEG, differentially-expressed genes.

(B) RNA-seq-based gene set enrichment analysis of pathways significantly upregulated in parental versus neratinib-resistant cells, both in the presence of neratinib. EMT, epithelial-to-mesenchymal transition.

(legend continued on next page)

Consistent with this analysis, we noted significant upregulation of genes associated with TORC1 signaling in 5637[NR] (enrichment score 0.45; q < 0.0001) and OVCAR8[NR] cells (enrichment score 0.3; q = 0.008) compared with parental cells (Figure 2D). Expression profiles of individual genes associated with TORC1 signaling in neratinib-treated parental and resistant cells are shown in Figure S2C. To confirm TORC1 activation in resistant cells, we performed immunoblot analysis on cells treated with increasing concentrations of neratinib (Figure 2E). EGFR, HER2, and HER3 phosphorylation was suppressed upon neratinib treatment, indicating sustained drug target inhibition. However, drug-resistant cells showed a striking increase in phosphorylation of TORC1 substrates such as p70 S6 kinase (S6K) and S6 compared with parental cells, which was sustained even in the presence of suprapharmacological concentrations of the TKI. To further support that S6K activation was mediated by TORC1, we performed an in-depth analysis of the pathway (Figure S2D). We noted increased phosphorylation of mTOR(S2448) and S6K at T389, a site exclusively phosphorylated by TORC1 (Magnuson et al., 2012). The 5637[NR] and OVCAR8[NR] cells retained expression of the founder HER2 mutation (Figure S2E) without acquired gain-of-function/gatekeeper mutations in HER2 (data not shown). Collectively, these data suggest ERBB receptor-independent activation of TORC1 in HER2-mutant cell lines that have acquired resistance to neratinib.

In addition, we developed neratinib-resistant breast cancer patient-derived xenografts (PDXs) through prolonged treatment of initially neratinib-sensitive ST1616B (HER2-amplified, HER2[D769Y]) PDXs (Figure 2F). Immunoblot analysis of tumor lysates revealed marked reduction in P-mTOR(S2448), P-AKT(S473), and P-ERK(T202/Y204) levels in neratinib-treated sensitive tumors (Figure 2G). However, neratinib treatment failed to suppress TORC1 activity in 4/4 independently derived neratinib-resistant tumors despite P-HER2 inhibition. Further, immunohistochemistry (IHC) analysis revealed reactivation of S6 phosphorylation in neratinib-resistant tumors compared with sensitive tumors (Figures 2H and S2F). Similarly, immunoblot and IHC analyses of intrinsically neratinib-resistant HER2[V842I] ST1456B triple-negative breast cancer PDXs showed maintenance of mTOR, AKT, S6K, and S6 phosphorylation in neratinib-treated tumors (Figures S2G–S2I and 2I).

Approximately 70% of HER2-mutant breast cancers are estrogen receptor positive (ER+) (cBioPortal.org). We generated neratinib resistance in ER+ MCF7 cells with knock-in HER2[V777L] mutation (Zabransky et al., 2015). MCF7[V777L] cells were cultured under estrogen-deprived conditions, in the presence of gradu-

ally increasing concentrations of neratinib until resistance was achieved (Figure S2J). HER2-activating mutations have been shown to promote endocrine resistance in ER+ metastatic breast cancers (Croessmann et al., 2019; Nayar et al., 2019). The growth rate of MCF7[V777L-NR] was higher than that of parental cells grown in the absence of estrogen (Figure S2K). To examine if MCF7[V777L-NR] still depended on ligand-independent ER activity, we used the ER antagonist fulvestrant. Compared with parental cells, the IC$_{50}$ of MCF7[V777L-NR] cells to the combination of neratinib/fulvestrant was >100-fold higher (Figure S2L). Insensitivity to neratinib/fulvestrant was associated with induction of P-mTOR(S2448) and P-S6(240) in MCF7[V777L-NR] cells (Figure S2M).

Collectively, these observations made in multiple neratinib-resistant models of diverse histological origins support TORC1 activation as a common node mediating neratinib resistance.

Genetic and Therapeutic Suppression of TORC1 Overcomes Resistance to Neratinib

To investigate if TORC1 activation is causal to neratinib resistance, we tested whether pharmacological suppression of TORC1 could restore sensitivity to neratinib in 5637[NR] and OVCAR8[NR] cells. TORC1 integrates signaling inputs from several pro-survival mitogenic pathways, including PI3K-AKT and MAPK. Thus, we tested the effect of combining neratinib with inhibitors of PI3Kα (alpelisib), TORC1 (everolimus), MEK1/2 (selumetinib), and AKT (MK-2206), and with the pan-PI3K inhibitor buparlisib to evaluate involvement of other PI3K isoforms. Our goal behind this drug screen was to identify drug combinations that abrogate neratinib resistance and to identify potential activators of TORC1 in the drug-resistant cells. While the combination of neratinib with alpelisib, selumetinib, buparlisib, or MK-2206 led to near complete blockade of S6 phosphorylation in parental cells, they only partially suppressed P-S6 levels in neratinib-resistant cells (Figures 3A and S3A). On the other hand, the combination of everolimus and neratinib induced robust inhibition of P-S6 in both 5637[NR] and OVCAR8[NR] cells. Next, we tested the effect of these drugs, either alone or with neratinib, on the viability of neratinib-resistant cells (Figures 3B and 3C). Consistent with the biochemical data, everolimus was far superior to PI3K or MEK inhibitors at restoring sensitivity to neratinib. These results suggest that PI3K or MAPK inhibitors only partially suppress TORC1 activation and, therefore, are not highly effective at reversing neratinib resistance.

To expand these observations, we tested the efficacy of TORC1 inhibition at overcoming neratinib resistance in breast

(C) Connectivity map analysis to identify drugs that could potentially reverse expression of resistance-associated genes. mTOR inhibitors are highlighted with red arrows.
(D) Enrichment plots for genes associated with TORC1 activation in parental versus neratinib-resistant cells, both in the presence of neratinib.
(E) Immunoblots of parental and neratinib-resistant 5637 and OVCAR8 cells treated with increasing concentrations of neratinib. After treatment for 24 h, whole-cell lysates were prepared and subjected to immunoblot analyses with the indicated antibodies.
(F) Generation of neratinib-resistant ST1616B (HER2-amplified, HER2[D769Y]) breast cancer PDXs as described in the STAR Methods. Mice with established ST1616B tumors were treated with vehicle (blue) or neratinib (40 mg/kg; green/red). Four sensitive (green) and resistant (black arrows) tumors were harvested for molecular analyses.
(G) Immunoblot analysis of neratinib-sensitive and -resistant ST1616B PDXs harvested 2 h after the last drug treatment.
(H) Representative P-S6 IHC images of tumors from (F); scale bar, 50 μm.
(I) Immunoblots of vehicle- and neratinib-treated de novo resistant ST1456B (HER2[V842I]) breast cancer PDXs. Tumors were harvested 1–2 h after the last drug treatment.
See also Figure S2.
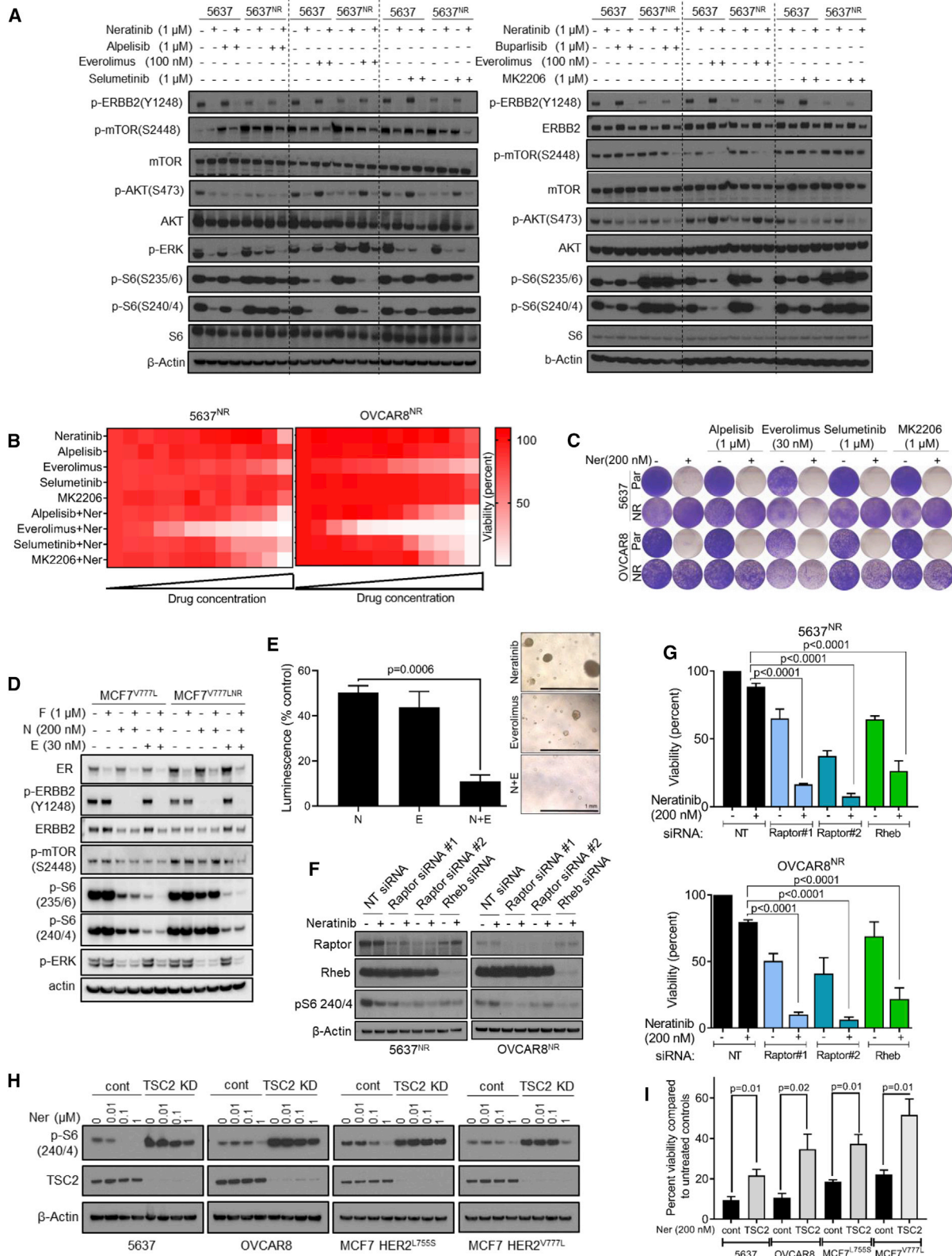
Figure 3. Genetic and Therapeutic Suppression of TORC1 Overcomes Resistance to Neratinib

(A) Immunoblot analysis of parental and neratinib-resistant 5637 cells treated with the indicated drug combinations for 24 h. Alpelisib (PI3Kα inhibitor), everolimus (TORC1 inhibitor), selumetinib (MEK1/2 inhibitor), buparlisib (pan-PI3K inhibitor), MK2206 (AKT inhibitor).

(legend continued on next page)

cancer cells and PDXs. The combination of neratinib and fulvestrant resulted in marked suppression of P-mTOR, P-S6, and P-ERK in parental MCF7^{V777L} cells (Figure 3D). On the other hand, TORC1 signaling in MCF7$^{V777L-NR}$ cells was completely refractory to neratinib/fulvestrant. The addition of everolimus robustly inhibited both P-S6 and P-ERK levels and also restored sensitivity to neratinib/fulvestrant (Figures 3D and S3B). Similarly, organoids established from neratinib-resistant ST1616B PDXs were exquisitely sensitive to neratinib/everolimus, but not to the single agent neratinib or everolimus (Figure 3E).

To further support TORC1 dependence, we genetically suppressed TORC1 activity in 5637^{NR} and OVCAR8^{NR} cells by knocking down the expression of critical positive regulators of TORC1 (Figures 3F and 3G). RAPTOR is a scaffolding protein of mTOR complex 1 that recruits key substrates such as S6K and 4EBP1 to the mTOR kinase (Hay and Sonenberg, 2004; Laplante and Sabatini, 2009). RHEB is directly upstream of TORC1 that, in its GTP-bound state, activates the mTOR kinase. Small interfering RNA (siRNA)-mediated knockdown of RAPTOR or RHEB led to near complete loss of P-S6 and viability of neratinib-treated 5637^{NR} and OVCAR8^{NR} cells, thereby supporting that TORC1 suppression restores sensitivity to neratinib. These findings were further corroborated by constitutively activating TORC1 in parental 5637, OVCAR8, and breast cancer MCF7 cells with isogenically incorporated HER2-activating mutations (MCF7^{L755S} and MCF7^{V777L}) (Figures 3H and 3I) (Zabransky et al., 2015). TSC2 is an integral component of the TSC1/2 complex, which negatively regulates TORC1 kinase function. Compared to 5637 and OVCAR8 cells, MCF7^{L755S} and MCF7^{V777L} cells showed a relatively modest growth suppression in response to neratinib due to an underlying $PIK3CA^{H1047R}$ mutation. Knockdown of TSC2 impaired neratinib-induced reduction in S6 phosphorylation and viability of parental 5637, OVCAR8, MCF7^{L755S}, and MCF7^{V777L} cells. On the other hand, inactivation of the TORC2 complex through gene silencing of RICTOR had no effect on P-S6 levels or the viability of neratinib-resistant cells (Figures S3C–S3E). Further, the combination of neratinib with the TORC1/2 inhibitor sapanisertib was equivalent to neratinib/everolimus at restoring neratinib sensitivity

(Figure S3F), suggesting that resistance to neratinib is primarily driven by TORC1.

Xenografts of parental 5637 and OVCAR8 cells established in nude mice were sensitive to neratinib (Figures S4A and S4B). Next, we tested the efficacy of neratinib ± everolimus against 5637^{NR} and OVCAR8^{NR} xenografts in vivo (Figures 4A–4G). Drug treatments were initiated when tumors reached an average volume of 200–250 mm^3 (5637^{NR}, ~3 months post-inoculation; OVCAR8^{NR}, ~5 weeks post-inoculation). Tumor growth was unaffected by neratinib, suggesting persistence of a drug-resistant phenotype in the absence of continuous drug exposure (Figures 4A, B, and E). Similarly, everolimus alone did not effectively suppress xenograft growth, suggesting that neratinib-resistant tumors were still dependent on mutant-HER2 signaling. However, the combination significantly arrested OVCAR8^{NR} tumor growth and led to marked regression of 5637^{NR} tumors. This anti-tumor effect was associated with downregulation of P-S6 levels in tumors treated with neratinib/everolimus compared with those treated with single-agent neratinib (Figures 4C, 4D, 4F, and 4G). Collectively, these data suggest that TORC1 inhibition could restore the sensitivity of 5637^{NR} and OVCAR8^{NR} cells to neratinib in vitro and in vivo.

RAS Hyperactivity Is Associated with TORC1 Activation and Neratinib Resistance in a Subset of *HER2*-Mutant Cancers

TORC1 integrates proliferative signals from several mitogenic pathways, including the PI3K-AKT and MAPK pathways. The partial sensitivity of 5637^{NR} and OVCAR8^{NR} cells to both PI3K inhibition and MEK1/2 inhibition (Figure 3A) prompted us to explore the effect of combined PI3K and MAPK blockade on TORC1 activation. For this purpose, we used the pan-PI3Ki buparlisib and the MEK1/2i trametinib. Treatment with everolimus (TORC1i) or with buparlisib/trametinib only partially suppressed P-S6 despite effective inhibition of their respective molecular targets, P-AKT(S473) and P-ERK(T202/Y204), by the combination (Figure 5A). The triple combination of buparlisib, trametinib, and neratinib completely suppressed P-S6 levels, thus phenocopying the effect of everolimus/neratinib. These data suggest that

(B) Heatmaps representing 12-point dose-response assays of 5637^{NR} and OVCAR8^{NR} cells treated with the indicated single agents or combinations. For single agents, cells were treated with increasing concentrations (3-fold) of the drug, up to 1 μM. For combination assays, all cells were treated with 1 μM neratinib and increasing concentrations of the second drug.

(C) Representative images of cells seeded in 12-well plates and treated with the indicated drug combinations; drugs and media were replenished every 72 h. When control cell monolayers reached ~90% confluency, they were stained with crystal violet and imaged.

(D) Immunoblot analysis of parental and neratinib-resistant MCF7^{V777L} cells treated with the indicated drugs for 24 h.

(E) Growth of organoids established from neratinib-resistant ST1616B (*HER2*^{D769Y}) breast cancer PDX. Organoids were treated with vehicle, neratinib (100 nM), everolimus (30 nM), or the combination. Viability was assessed 6 days later by measuring ATP levels and normalized to vehicle-treated control. Each bar represents mean ± SEM from three independent experiments. P value, and Student's t test. Representative images of organoids from each treatment group are shown on the right; scale bar, 1 mm.

(F) Immunoblot analysis of neratinib-treated 5637^{NR} and OVCAR8^{NR} cells transfected with the indicated siRNAs.

(G) Viability of neratinib-treated cells transfected with the indicated siRNAs. When control cells reached ~90% confluency, cells were trypsinized and counted using a Coulter counter. Each bar represents mean ± SEM from three independent experiments. P values, and one-way ANOVA.

(H) Immunoblot analysis of lysates from 5637, OVCAR8, MCF7^{L755S}, and MCF7^{V777L} cells stably transfected with *TSC2* short hairpin RNA (shRNA) or empty-vector control. Cells were treated with increasing concentrations of neratinib; 24 h later, cell lysates were prepared and tested by immunoblot with the indicated antibodies. MCF7^{L755S} and MCF7^{V777L} cells were tested under estrogen-free conditions.

(I) Viability of 5637, OVCAR8, MCF7^{L755S}, and MCF7^{V777L} cells transfected with *TSC2* shRNA or empty vector and treated with neratinib. Drug and media were replenished every 72 h. MCF7^{L755S} and MCF7^{V777L} cells were treated with neratinib under estrogen-free conditions. When control cells reached ~90% confluency, monolayers were trypsinized and cell number was measured using a Coulter counter. Each bar represents mean cell viability ± SEM from three independent experiments. P values, and Student's t test.

See also Figure S3.
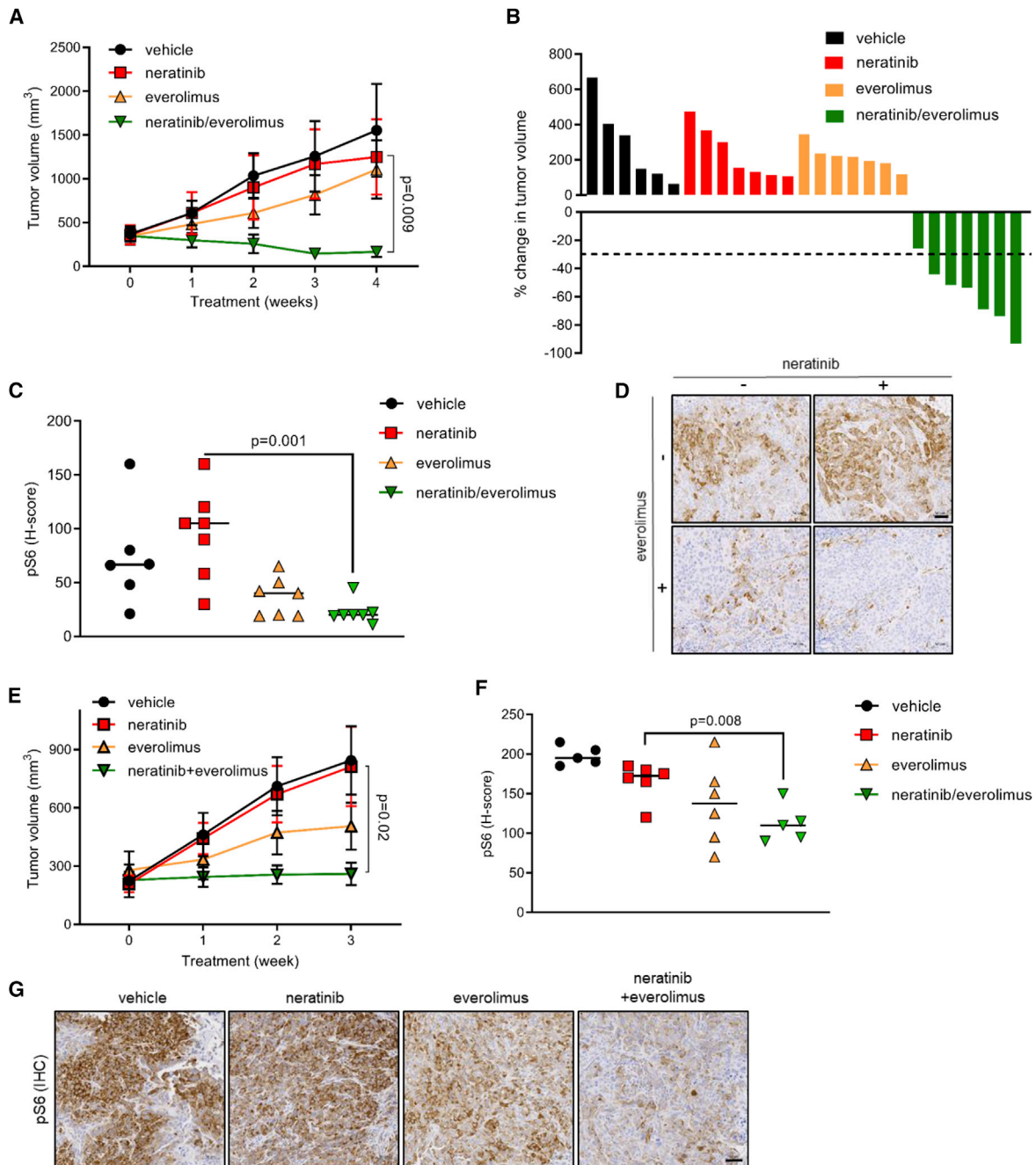
Figure 4. Neratinib in Combination with Everolimus Suppresses Growth of Established Neratinib-Resistant *HER2*-Mutant Xenografts

(A) Growth of 5637[NR] tumors treated with vehicle, neratinib (40 mg/kg), everolimus (5 mg/kg), or both drugs. Each data point represents mean tumor volume in mm^3 ± SEM (n ≥ 6 mice per arm). P value, and Student's t test.

(B) Percentage change in volume of individual 5637[NR] tumors in each treatment arm shown in (A).

(C) H-score quantification (described in STAR Methods) of P-S6 levels in 5637[NR] tumors shown in (A). Horizontal line indicates the median. P value, and Student's t test.

(D) Representative images from (C); scale bar, 50 μm.

(E) Growth of established OVCAR8[NR] xenografts treated with vehicle, neratinib (40 mg/kg), everolimus (5 mg/kg), or both drugs. Each data point represents mean tumor volume in mm^3 ± SEM (n ≥ 5 mice per group). P value, and Student's t test.

(F) P-S6 H-scores based on IHC analysis of OVCAR8[NR] tumors shown in (E). Horizontal line indicates the median. P value, and Student's t test.

(G) Representative images from (F); scale bar, 50 μm.

See also Figure S4.
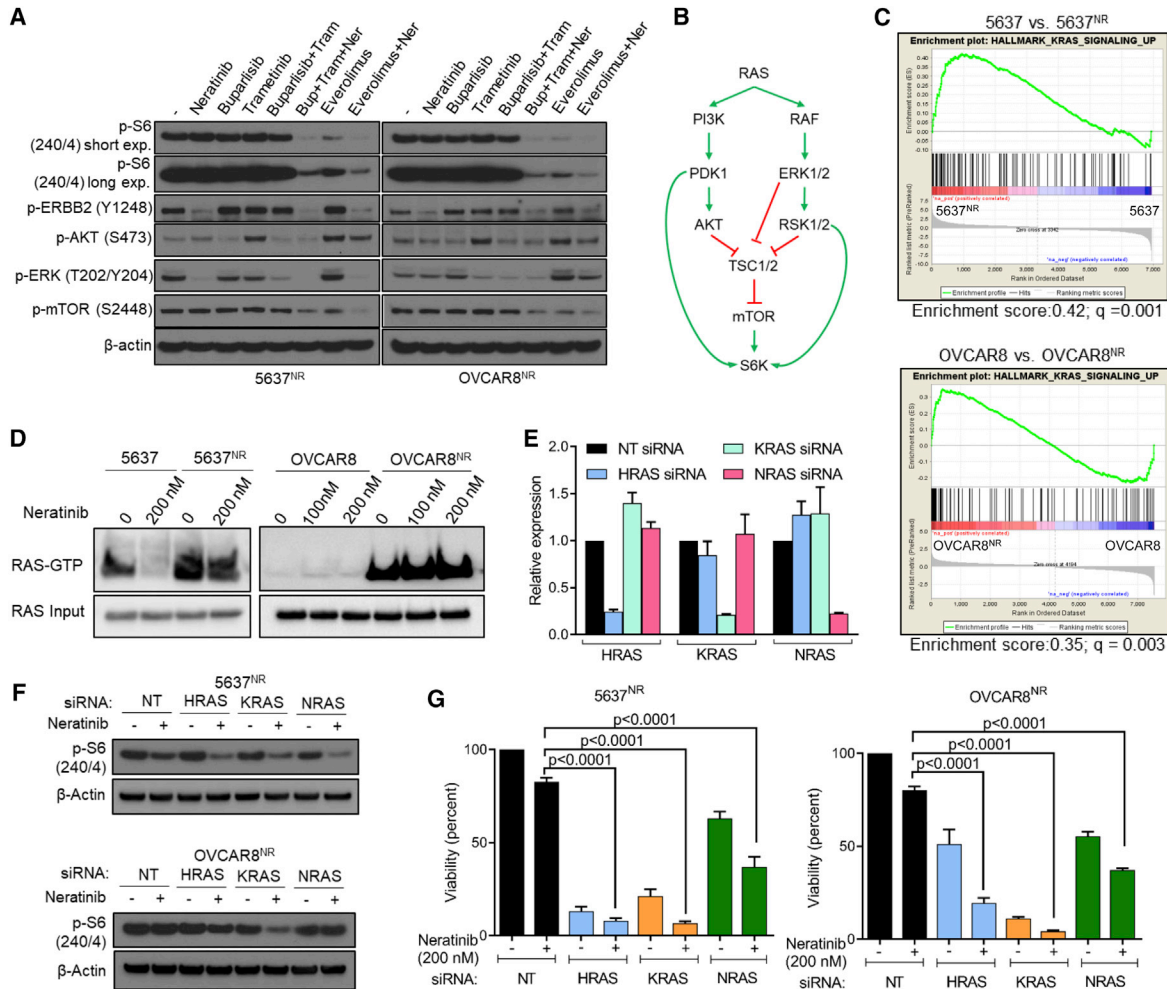
Figure 5. RAS Hyperactivity Is Associated with Increased TORC1 Activity and May Mediate Neratinib Resistance

(A) Immunoblot analysis of 5637[NR] and OVCAR8[NR] cells treated for 24 h with neratinib, buparlisib, trametinib, or everolimus.

(B) Schematic representation of RAS-mediated TORC1 activation.

(C) Enrichment plots for RAS pathway-related genes in neratinib-treated parental cells versus neratinib-resistant cells.

(D) Active-RAS pull-down assay in parental and neratinib-resistant 5637 and OVCAR8 cells treated with neratinib for 6 h.

(E) mRNA levels by qPCR of RAS isoforms in 5637[NR] cells ± siRNAs against HRAS, KRAS, or NRAS. Each bar represents mean ± SEM from three independent experiments.

(F) Immunoblots of neratinib-treated 5637[NR] and OVCAR8[NR] cells transfected with siRNAs against HRAS, KRAS, or NRAS.

(G) Growth assay of neratinib-treated cells transfected with the indicated siRNAs. Each bar represents mean ± SEM from three independent experiments. P value, and one-way ANOVA.

See also Figure S5.

in 5637[NR] and OVCAR8[NR] cells, both PI3K and MAPK axes work in unison to promote TORC1 activity. RAS is known to modulate mTOR activity through simultaneous activation of both PI3K and MAPK pathways (Figure 5B) (Shaw and Cantley, 2006). Thus, we investigated RAS pathway activation status in the RNA-seq data. We noted significant enrichment of the RAS pathway gene set in both 5637[NR] and OVCAR8[NR] cells, which was sustained in the presence of neratinib (Figure 5C). To confirm these observations, we compared active RAS levels in parental and neratinib-resistant cells. For this purpose, we performed a RAS activity assay, which utilizes the RAS binding domain (RBD) of RAF-1 to pull down active RAS molecules from whole-cell lysates. Compared with parental cells, we found a striking increase in active RAS

levels in both 5637[NR] and OVCAR8[NR] cells, which was sustained in the presence of a clinically relevant dose of 200 nM neratinib (Figure 5D). Expression profiles of individual genes associated with RAS signaling in neratinib-treated parental and resistant cells are shown in Figure S5A. Each RAS siRNA achieved ~80% reduction in the expression of the target RAS isoform without affecting the expression of other isoforms (Figure 5E). siRNA-mediated knockdown of HRAS, KRAS, and NRAS isoforms in neratinib-treated 5637[NR] and OVCAR8[NR] cells resulted in inhibition of P-S6 and reversal of neratinib resistance (Figures 5F and 5G), thus suggesting RAS-dependent TORC1 hyperactivity and drug resistance. In order to identify a potential mechanism for RAS activation, we performed whole-exome
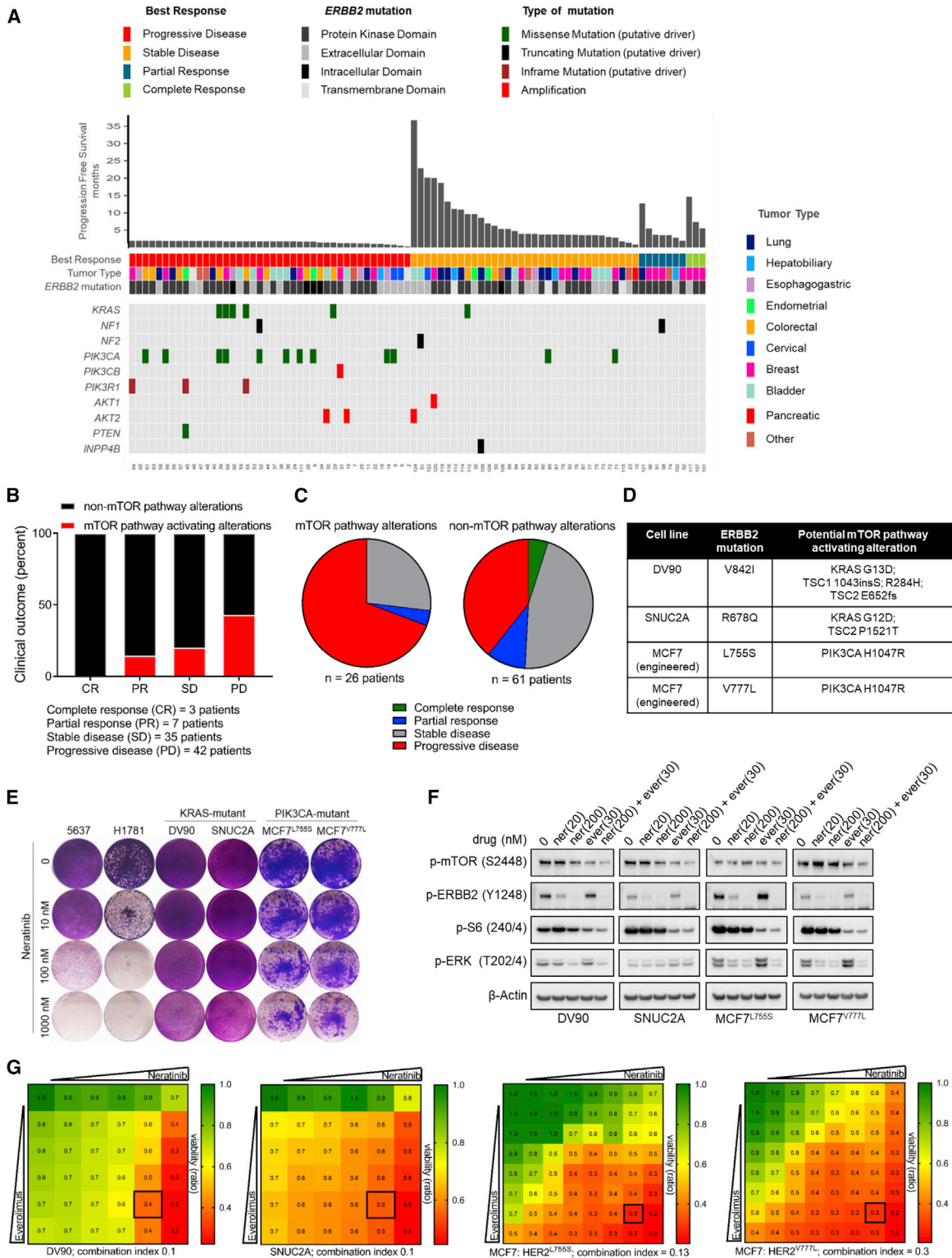
Figure 6. mTOR Pathway-Activating Co-mutations in *HER2*-Mutant Cancers Are Associated with Clinical Resistance to Neratinib

(A–C) Clinical outcome of patients enrolled in the SUMMIT trial of neratinib based on mTOR pathway-associated alterations in their tumors; depicted as a tile plot (A), percentage distribution (B), and pie chart (C) (cBioPortal SUMMIT - Nature 2018, http://www.cbioportal.org/study?id=summit_2018). Mutations were classified as "mTOR-activating alterations" or "non-mTOR-pathway alterations" as described in the STAR Methods and Table S1.

(D) Mutation status of *HER2* and other key cancer genes in *HER2*-mutant cell lines.

(legend continued on next page)

sequencing on parental and neratinib-resistant cells. DNA sequencing identified an acquired $RASA2^{G787X}$ truncating mutation in 5637^{NR} cells. RASA2 is a RAS GTPase-activating protein (GAP) that negatively regulates RAS function by catalyzing its conversion to an inactive GDP-bound form. Loss-of-function missense and truncating mutations in $RASA2$ occur in melanoma and RASopathy syndromes, including residues in close proximity to the G787 site (Arafeh et al., 2015; Chen et al., 2014; Halaban and Krauthammer, 2016). Such RASA2-inactivating alterations have been shown to exert haploinsufficient and dominant negative effects on wild-type (WT) protein function (Arafeh et al., 2015; Chen et al., 2014). To investigate whether RASA2 downregulation is causal to TORC1 hyperactivation, we silenced $RASA2$ expression in parental 5637 cells. Knockdown of $RASA2$ abrogated neratinib-induced suppression of mTOR phosphorylation (Figure S5B). Consistent with these data, overexpression of WT RASA2 in 5637^{NR} cells suppressed TORC1 hyperactivity and restored neratinib sensitivity (Figures S5C–S5E). This resensitization was accompanied by decreased RAS-GTP levels (Figure S5C) and downregulation of P-AKT(S473), P-S6K(T389), and P-S6(240) levels in neratinib-treated 5637^{NR} RASA2 cells. Unlike 5637^{NR} and $OVCAR8^{NR}$ cells, TORC1 activation in breast cancer $MCF7^{V777L-NR}$ cells was not associated with an upregulation in RAS function (Figure S5F), suggesting that different $HER2$-mutant cancer types may adopt distinct resistance mechanisms that converge on TORC1 signaling.

mTOR Pathway Co-mutations in *HER2*-Mutant Cancers Are Associated with Clinical Resistance to Neratinib

We next tested whether the presence of co-mutations in the mTOR pathway influenced the clinical response to neratinib in patients with $HER2$-mutant cancers enrolled in the phase II SUMMIT trial. For this purpose, we accessed DNA sequencing data (MSK-IMPACT panel; 410 genes) on pre-treatment tumors from 141 patients with multiple cancer types (http://www.cbioportal.org/study?id=summit_2018, SUMMIT - Nature 2018) (Hyman et al., 2018). Table S1 provides a list of mutations that were deemed mTOR pathway-activating alterations in our analysis. We noted an enrichment of somatic alterations associated with aberrant mTOR activation in patients exhibiting primary resistance to neratinib (Figures 6A–6C). The majority of patients whose cancers carried activating mutations in RAS ($KRAS$), loss-of-function alterations in negative regulators of RAS ($NF1$), gain-of-function alterations in the PI3K axis ($PIK3CA$, $PIK3CB$, $AKT1$, and $AKT2$), and inactivating mutations in suppressors of PI3K function ($PIK3R1$, $PTEN$, and $INPP4B$) did not derive clinical benefit from neratinib. In addition, we found 4 patients with missense mutations in $RPTOR$ (3 of 4 exhibited rapid progressive disease), 1 patient with a $TSC2$ missense mutation (with a short progression-free survival [PFS] of 4.7 months), 1 patient with a

$RHEB$ missense mutation (PFS 1.7 months), and 1 patient each with an $MTOR$ missense mutation (PFS 3.4 months) and a truncating mutation (PFS 2.1 months). However, the oncogenic functions of these $RPTOR$, $RHEB$, $TSC2$, and $MTOR$ mutations remain uncharacterized and, thus, these mutations were not considered to be mTOR activating in our analysis. Patients with tumors harboring $BRAF$ mutations also exhibited a poor response to neratinib (3 of 4 progressed). Even though BRAF-activating mutations have been shown to activate mTOR signaling (Corcoran et al., 2013; Faber et al., 2014; Prabowo et al., 2014), such mutations mediate their oncogenic effects primarily through MEK/ERK (Solit et al., 2006) and, hence, were not considered as mTOR pathway alterations in this analysis. Outcome analysis of breast cancer, which was the most responsive tumor subtype in the SUMMIT trial, showed that 6/7 patients with progressive disease harbored a TORC1-activating co-mutation in their tumors (5 $PIK3CA$, 1 $PIK3R1$) (Figure S6A).

To functionally validate these findings, we tested neratinib sensitivity of $HER2$-mutant cell lines bearing co-mutations in components of the mTOR pathway that were most frequently observed in the clinical cohort (Figure 6D). $HER2$-mutant $DV90^{V842I}$ lung cancer, $SNUC2A^{R678Q}$ colorectal cancer, and $MCF7^{L755S}$ and $MCF7^{V777L}$ breast cancer cells with either $KRAS$ or $PIK3CA$ co-mutation were intrinsically resistant to neratinib (Figure 6E). This was in stark contrast to the exquisite neratinib sensitivity of 5637^{S310F} and $H1781^{G776>VC}$ $HER2$-mutant cell lines lacking $KRAS$- or $PIK3CA$-activating mutations. In line with these findings, $PIK3CA$-mutant HCI-003 $HER2^{G778\_P780dup}$ breast cancer PDXs showed only a modest growth delay in response to single-agent neratinib, which was associated with maintenance of TORC1 activity (Figures S6B–S6E). Immunoblot analysis of DV90, SNUC2A, $MCF7^{L755S}$, and $MCF7^{V777L}$ cells revealed sustained P-S6 levels in the presence of neratinib, consistent with the lack of an effect on cell viability (Figure 6F). Although single-agent everolimus suppressed activation of the S6K targets P-mTOR(S2448) and P-S6(240/4), P-ERK levels remained high. On the other hand, treatment with neratinib/everolimus resulted in robust blockade of both TORC1 and MAPK. To further demonstrate that the combination of neratinib/everolimus can overcome intrinsic resistance to neratinib, we assessed drug interaction using the Chou-Talalay method (Chou, 2010), where a combination index (CI) < 1 indicates synergy; CI = 1 indicates additive effect, and CI > 1 indicates antagonism (Figure 6G). Combination studies using increasing concentrations of neratinib and everolimus demonstrated striking synergy between these agents at inhibiting the growth of DV90 (CI < 0.1), SNUC2A (CI = 0.1), $MCF7^{L755S}$ (CI = 0.13), and $MCF7^{V777L}$ (CI = 0.3) cells.

In order to rule out any confounding effects from $TSC1/TSC2$ or other co-mutations present in these intrinsically resistant cells, we studied the effects of aberrant activation of KRAS and

(E) Crystal violet-stained monolayers of 5637, H1781, DV90, SNUC2A, $MCF7^{L755S}$, and $MCF7^{V777L}$ cells seeded in 12-well plates and treated with the indicated concentrations of neratinib. Cell monolayers were stained and imaged when vehicle-treated controls reached ∼90% confluency.

(F) Immunoblot analysis of DV90, SNUC2A, $MCF7^{L755S}$, and $MCF7^{V777L}$ cells treated with indicated concentrations of neratinib, everolimus, or both drugs for 24 h.

(G) Viability assay to test synergy between neratinib and everolimus. Cells were treated with increasing concentrations of each drug alone or both drugs every 72 h until vehicle-treated controls reached ∼90% confluency. Cell monolayers were then stained with crystal violet; staining intensities were quantified colorimetrically, and combination indices were determined using the Chou-Talalay test. Numbers inside each box indicate the ratio of viable treated cells to untreated cells from three independent experiments.

See also Figure S6 and Table S1.
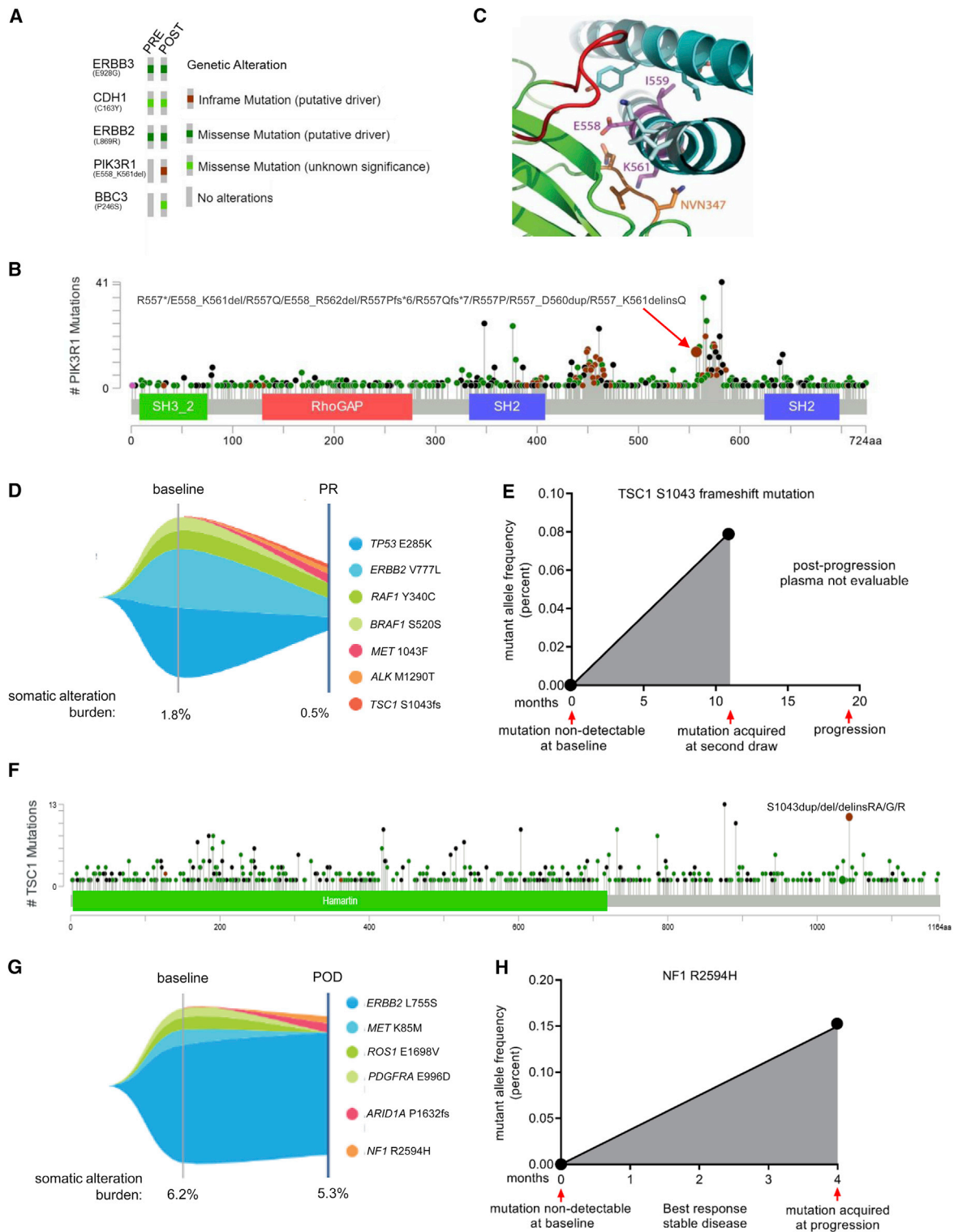
Figure 7. Acquired mTOR Pathway Mutations in Patients Progressing on Neratinib

(A) OncoPrint of mutations detected by targeted capture NGS of archival primary tumor and a skin metastasis biopsied at the time of progression on neratinib.

(B) Lollipop plot depicting the prevalence of *PIK3R1* mutations queried in 1,599 patients' tumors in cBioPortal.

(C) Structure of p85α iSH2 (cyan ribbon) bound to p110α (green ribbon). Amino acid residues 558–561 (deleted in *PIK3R1*[558-561 del]; EIDK, shown as magenta sticks) lie within the iSH2 helical domain of p85α (PDB: 4OVU). E558 and I559 residues interact with the neighboring p85α helix (cyan stick), and K561 interacts

(legend continued on next page)

PIK3CA on neratinib-sensitive cells. Introduction of $KRAS^{G12V}$ or $PIK3CA^{H1047R}$ in $HER2$-mutant 5637 and OVCAR8 cells resulted in near complete resistance to neratinib (Figures S6F–S6H). This effect on cell viability was associated with robust induction of S6K, S6, and ERK phosphorylation that was sustained in the presence of neratinib (Figures S6I and S6J). Concurrent neratinib/everolimus treatment suppressed TORC1 signaling and restored sensitivity to neratinib (Figures S6K–S6O). Collectively, these data suggest that the combination of neratinib with a TORC1 inhibitor is effective at arresting $HER2$-mutant cancers with $KRAS$- or $PIK3CA$-activating co-mutations.

Amplification of $AKT1$ and $AKT2$ genes was also noted in a subset of patients that derived lesser benefit from neratinib. In agreement with these clinical findings, overexpression of AKT1 or AKT2 resulted in constitutive activation of AKT, S6K, and S6 and resistance to neratinib (Figures S6P and S6Q). Similarly, we validated loss-of-function mutations in tumor suppressors such as $PTEN$, $NF1$, and $NF2$ through siRNA-mediated gene silencing. Knockdown of $PTEN$, $NF1$, or $NF2$ expression enhanced mTOR(S2448) phosphorylation and attenuated neratinib sensitivity of $HER2$-mutant cells (Figures S6R and S6S).

mTOR Pathway Mutations Are Acquired in $HER2$-Mutant Cancers that Progress on Neratinib

Finally, we determined the prevalence of mTOR pathway alterations in tumors that progressed after an initial clinical response to neratinib. Of 14 post-progression biopsies that were available at the time of this analysis, 3/14 (21%) had acquired mutations in the mTOR pathway that were absent at treatment onset. DNA sequencing (384 genes, Foundation One) of a progressing skin metastasis in a patient with breast cancer harboring $HER2^{L869R}$ revealed $PIK3R1^{558-561\ del}$ and $BBC3^{P246S}$ mutations (Figures 7A and S7A). BCL2 binding component 3 (BBC3) is a proapoptotic BH3-only protein (Han et al., 2001), but there are no reports of the P246S substitution in the cBioPortal (n > 72,000 samples) or COSMIC (n > 35,000 samples) database. The phosphoinositide 3-kinase regulatory subunit p85α ($PIK3R1$) is a negative regulator of p110α ($PIK3CA$) and is frequently mutated in cancer (Cheung and Mills, 2016). The $PIK3R1^{558-561}$ deletion is reported to be a statistically significant mutation hotspot in cBioPortal (Figure 7B). The nSH2 and iSH2 domains of p85α interact with helical and C2 domains of p110α, respectively, to repress its catalytic function (Burke et al., 2012; Miled et al., 2007). Thus, we next performed structural analysis to determine if deletion of residues 558–561 (EIDK) in the iSH2 domain of p85α would disrupt the inhibitory interaction with p110α and render the kinase constitutively active. In Figure 7C, we highlight the interaction between p110α and p85α surrounding the deletion site (Huang et al., 2007). Deleted residues in p85α are shown in

magenta and corresponding binding domains in p110α are shown in green. Specifically, lysine^{561} of p85α interacts with a loop (residues N345–N347, shown in orange) in the p110α C2 domain. Disruption of this C2-iSH2 domain interface has been shown to constitutively activate PI3K (Wu et al., 2009). Further, deletion of these residues in p85α would presumably result in loss of a turn in the iSH2 helix and thereby disrupt the alignment of residues that are C-terminal to the deletion. These C-terminal residues interact with another loop from the p110α C2 domain (red), whose deletion was previously shown to hyperactivate PI3K (Croessmann et al., 2018). To confirm these findings, we interrogated the mutation impact prediction tool in COSMIC, which predicts the functional consequences of missense mutations based on the FATHMM-MKL algorithm (Shihab et al., 2015). For each query mutation, the algorithm assigns a score ranging from 0 to 1, with scores ≤0.5 indicating neutral variation and scores ≥0.7 indicating a pathogenic mutation. Consistent with the results rendered by the structural analysis above, the FATHMM algorithm predicted a missense mutation in D560, one of the deleted residues in $PIK3R1^{558-561\ del}$, to be highly pathogenic (score 0.99). $PIK3R1^{D560}$ mutations have been previously described as hypomorphic in nature due to their impaired ability to repress p110α, resulting in increased PI3K signaling, anchorage- and growth factor-independent growth, and tumorigenesis (Cheung and Mills, 2016; Jaiswal et al., 2009; Sun et al., 2010; Wu et al., 2009). Of note, these transforming properties of $PIK3R1^{D560}$ were shown to be sensitive to PI3K/TORC1 blockade (Jaiswal et al., 2009; Wu et al., 2009).

Next-generation sequencing (NGS) of plasma cell-free DNA (cfDNA; Guardant360) in a patient with $HER2^{V777L}$ breast cancer progressing on neratinib revealed ALK^{M1290T}, MET^{S1043F}, and $TSC1^{S1043}$ frameshift mutations that were not detected at baseline (Figures 7D, 7E, and S7B). We found only one case with the ALK^{M1290T} mutation in cBioPortal (n = 1,164) and no reports on the MET^{S1043F} mutation in cBioPortal or COSMIC. TSC1 is an integral part of the TSC1/2 complex that negatively regulates TORC1 activity (Laplante and Sabatini, 2009). Indels, substitutions, and duplications at S1043 in $TSC1$ have been noted (Figure 7F), and such alterations are predicted to be pathogenic (FATHMM score 0.87; COSMIC). Germline $TSC1^{S1043G}$ mutation was also associated with one case of hereditary cancer-predisposing syndrome (ClinVar). The patient had a partial response to neratinib at the time at which the $TSC1^{S1043}$ frameshift mutation was detected at a low allele frequency of 0.08%. Eight months later, the patient progressed on neratinib. The plasma sample drawn at the time of radiological progression was non-evaluable, and we were therefore unable to determine $TSC1^{S1043fs}$ allele frequency at progression. Further, interrogation of the mutation profiles of $HER2$-mutant cells in the Cancer Cell Line

---

with the C2 domain loop of p110α (345-NVN-347, orange stick). p85α residues that are C-terminal to the deleted region (light cyan stick) interact with residues from another p110α C2 loop (red).

(D) Tumor mutations identified by NGS of plasma cfDNA in a patient with breast cancer treated with neratinib for 11 months. Partial response denoted as PR.

(E) Variant allele fraction of $TSC1^{S1043}$ frameshift mutation in plasma cfDNA at baseline and during the course of neratinib treatment.

(F) Lollipop plot of $TSC1$ mutations queried in 1,168 samples in cBioPortal.

(G) Tumor mutations identified by NGS of plasma cfDNA in a patient with breast cancer that developed acquired resistance to neratinib. Progressive disease denoted as POD.

(H) Variant allele fraction of $NF1^{R2594H}$ at baseline and at disease progression on treatment.

See also Figure S7.

Encyclopedia (Broad Institute) revealed TSC1 1,043_1044insS in DV90 cells (with HER2^{V842I}), which are intrinsically resistant to neratinib (Figure 6E). Of note, the combination of neratinib/everolimus reversed neratinib resistance in DV90 cells (Figures 6F and 6G). To functionally characterize the TSC1^{S1043fs} mutation, we transduced HER2-mutant cells with WT or mutant TSC1. OVCAR8 cells stably expressing TSC1^{S1043fs} were resistant to neratinib-induced suppression of P-mTOR (S2448) and P-S6 (240/4) compared with those expressing WT TSC1 (Figure S7C). Consistent with these results, TSC1^{S1043fs} expression attenuated the sensitivity of OVCAR8 cells to neratinib (Figure S7D). The relative resistance of mutant TSC1 to neratinib-induced suppression of TORC1 signaling and growth suggests that the S1043 frameshift mutation abrogates the ability of TSC1 to inhibit TORC1. The combination of neratinib with the allosteric inhibitor of TORC1 everolimus was able to overcome the drug resistance effect of the TSC1^{S1043fs} loss-of-function mutation (Figure S7E).

Serial liquid biopsies on another patient with HER2^{L755S} breast cancer detected an acquired NF1^{R2594H} mutation at progression on neratinib (Figures 7G, 7H, and S7F). NF1 acts as a tumor suppressor by promoting GTP hydrolysis of RAS and inactivating RAS signaling (Bollag et al., 1996). Overall, we found 9 cases with an R2594 missense mutation (GENIE, cBioPortal, and COSMIC), of which 5 had the R2594H substitution. NF1^{R2594H} is predicted to be pathogenic (FATHMM score 0.99, pathogenic; COSMIC), and importantly, this mutation has been noted in patients with hereditary syndromes, including one patient with type I neurofibromatosis (ClinVar). Based on cfDNA analysis, this patient had also acquired a previously unreported ARID1A^{P1632fs} mutation at progression.

DISCUSSION

Gain-of-function mutations in the HER2 gene promote oncogenesis and have been shown to be sensitive to HER2-directed therapies in pre-clinical studies (Bose et al., 2013; Croessmann et al., 2019; Kavuri et al., 2015; Perera et al., 2009). HER2 inhibitors, including neratinib, afatinib, and poziotinib, have yielded favorable responses in a subset of patients with HER2-mutant cancers (Hyman et al., 2018; Lai et al., 2019; Li et al., 2018; Ma et al., 2017; Robichaux et al., 2018). The development of HER2^{T798I} gatekeeper mutations in HER2-mutant tumors that progressed on neratinib further suggests an oncogenic driver role for HER2 mutations (Hanker et al., 2017; Ma et al., 2017). However, clinical responses to neratinib and other HER2-targeted therapies are heterogeneous and often short-lived, suggesting that neratinib monotherapy might not be an effective approach to treating HER2-mutant cancers. Thus, successful treatment of HER2-mutant cancers would require identification of molecular drivers of de novo and acquired resistance and, on that basis, implementation of effective treatment combinations.

In this study we identified hyperactivation of TORC1 as a potentially actionable mechanism driving primary and secondary resistance to neratinib in HER2-mutant cancers. The TORC1 complex is an important downstream effector of signaling pathways commonly perturbed in cancers and has been previously implicated as an escape mechanism in ERBB receptor-targeted therapies. Combined inhibition of the mTOR-HER2 axes has

been shown to restore sensitivity to anti-HER2 agents in lapatinib- and trastuzumab-resistant HER2+ breast cancers (Eichhorn et al., 2008; Garcia-Garcia et al., 2012; O'Brien et al., 2014). Similarly, EGFR$^{\Delta E746-A750+T790M}$ mouse lung tumors that are resistant to the combination of afatinib/cetuximab exhibit strikingly elevated TORC1 activity (Pirazzoli et al., 2014). Further, DNA sequencing of EGFR-mutant tumors, collected pre- and post-progression on EGFR TKIs, revealed acquisition of a novel MTOR^{E2914K} mutation that was causally linked to erlotinib resistance (Yu et al., 2018). Combined inhibition of HER2 and TORC1 in neratinib-sensitive HER2-mutant cells is superior to HER2 inhibition alone, also suggesting dependence of HER2-mutant cancers on TORC1 signaling (Croessmann et al., 2019). Consistent with these pre-clinical findings, the combination of neratinib plus temsirolimus was demonstrated to have a greater overall response rate, clinical benefit rate, and PFS compared to single-agent neratinib in a randomized phase II study of patients with advanced HER2-mutant lung cancers (Gandhi et al., 2016). The addition of temsirolimus was well tolerated, with comparable incidences of grade 3 diarrhea (12% versus 14%). Collectively, these data suggest that the subtle dependence on the mTOR axis gets hardwired as an escape mechanism as HER2-mutant cancers evolve under the selection pressure of HER2 inhibitors. In this study, we show that pharmacological and genetic suppression of TORC1 resulted in near complete restoration of neratinib sensitivity. The combination of neratinib and everolimus resulted in marked suppression or regression of neratinib-resistant tumors in vivo, without associated toxicities. Finally, constitutive activation of TORC1 in parental, drug-sensitive cells abrogated their sensitivity to neratinib.

We noted only partial suppression of P-S6 and viability of neratinib-resistant cells treated with PI3K, AKT, or MEK1/2 inhibitors. On the other hand, simultaneous inhibition of PI3K/MAPK/HER2 signaling was equivalent to TORC1/HER2 inhibition, suggesting involvement of an upstream regulator of both PI3K and MAPK in neratinib resistance. In line with these findings, we noted significant upregulation of RAS activity in 5637^{NR} and OVCAR8^{NR} neratinib-resistant cells. RAS GTPases undergo oncogenic activation in ~25% of cancers through mechanisms including mutations in their GTP-binding domain, downregulation of RAS-inactivating GAP proteins, and/or RTK overexpression (Castellano and Downward, 2011). Activated RAS mediates its mitogenic effects mainly through the RAF/MEK/ERK and PI3K/AKT effector pathways. RAS-GTP binds to the RBD in the p110 catalytic subunits of PI3K, leading to its activation (Rodriguez-Viciana et al., 1994). Disruption of the RAS-PI3K interaction by mutating critical amino acid residues within the RBD of p110α abrogates KRAS- and HRAS-induced transformation (Gupta et al., 2007).

We found RAS upregulation to be causally associated with TORC1 hyperactivity and neratinib resistance in a subset of HER2-mutant models. This is consistent with other reports of TORC1 activation in RAS-driven cancers and the use of P-S6 levels as a biomarker of response to treatment. A subset of mutant-BRAF melanomas that progressed on BRAF, MEK, and CDK4/6 inhibitors were shown to acquire gain-of-function mutations in NRAS with a concomitant increase in tumor P-S6 levels (Teh et al., 2018). In vivo modeling of NRAS-driven MEKi + CDK4/6i resistance showed that the addition of the

TORC1/2 kinase inhibitor AZD2019 reversed drug resistance. Similarly, Corcoran et al. reported that *BRAF*-mutant cancers and cell lines that are recalcitrant to BRAF inhibitors maintain high P-S6 levels despite P-ERK suppression (Corcoran et al., 2013). Similarly, NF1 and NF2 tumor suppressors have been shown to promote TORC1 activation (Dasgupta et al., 2005; James et al., 2009; Johannessen et al., 2005).

For the analysis of primary resistance to neratinib in *HER2*-mutant cancers, we considered oncogenic aberrations of members of the RAS-PI3K axis as mTOR-activating alterations. We noted that patients with cancers harboring co-mutations that activate mTOR responded poorly to neratinib. Since we did not notice any new PI3K pathway mutations in 5637^{NR} and $OVCAR8^{NR}$ cells, we speculated that different cancer types may rely on distinct mechanisms to activate TORC1 signaling. For instance, in the SUMMIT trial, *HER2*-mutant breast cancers frequently harbor *PIK3CA* mutations, whereas colorectal cancers often carry *KRAS* co-mutations. Consistent with these clinical associations, *HER2*-mutant cell lines bearing *KRAS* or *PIK3CA* co-mutations were intrinsically resistant to neratinib. Combined treatment with neratinib/everolimus completely suppressed both P-S6 and P-ERK and reversed resistance to neratinib in these cells. In line with these findings, subgroup analysis of phase III BOLERO-1 and BOLERO-3 trials in patients with advanced HER2+ breast cancers indicated improved PFS benefit with everolimus in cases with *PIK3CA* mutations, *PTEN* loss, or hyperactive PI3K pathway (Andre et al., 2016). These findings suggest that everolimus could be clinically active in treating HER2-driven cancers with PI3K pathway alterations.

Finally, we noted acquisition of mTOR pathway mutations in 3 of 14 (21%) patients that progressed on neratinib after an initial favorable response. These results are reminiscent of other studies where tumors that escape a targeted therapy acquire mutations in the same drug target or pathway initially blocked by the respective therapy. For example, clinical resistance to first-generation EGFR inhibitors in *EGFR*-mutant lung cancers include on-target alterations such as the T790M gatekeeper mutation (~50%), compensatory bypass mechanisms such as *MET* amplification (~20%), and *HER2* amplification (~8%) (Camidge et al., 2014), all of which reactivate downstream signaling.

In conclusion, we propose that the combination of TORC1 inhibitors with neratinib is worthy of clinical investigation in a molecularly guided trial of *HER2*-mutant cancers with *de novo* or acquired mTOR pathway mutations.

STAR★METHODS

Detailed methods are provided in the online version of this paper and include the following:

AUTHOR CONTRIBUTIONS

Conceptualization, D.R.S., A.B.H., and C.L.A.; Methodology, D.R.S., A.G.Z., H.W., P.G.E., Y.G., A.B.H., Q.L., L.N.K., and C.L.A.; Data Acquisition and Analysis, D.R.S., A.G.Z., H.W., P.E.G., A.S., M.H.R., D.Y., K.M.L., L.F., Y.G., Q.L., L.N.K., M.R.B., T.D., J.K., A.B.H., and C.L.A.; Writing, D.R.S., A.B.H., A.G.Z., H.W., P.G.E., A.S., K.M.L., L.F., Y.G., Q.L., L.N.K., R.E.C., A.S.L., R.B., A.A., and C.L.A.; Resources, D.R.S., A.B.H., M.J.W., R.E.C., A.S.L., R.B., A.A., and C.L.A.; Administrative/Technical Support, T.D., J.K., and C.L.A.; Study Supervision, D.R.S., A.B.H., and C.L.A.

DECLARATION OF INTERESTS

REFERENCES

Andre, F., Hurvitz, S., Fasolo, A., Tseng, L.M., Jerusalem, G., Wilks, S., O'Regan, R., Isaacs, C., Toi, M., Burris, H., et al. (2016). Molecular alterations and everolimus efficacy in human epidermal growth factor receptor 2-overexpressing metastatic breast cancers: combined exploratory biomarker analysis from BOLERO-1 and BOLERO-3. J. Clin. Oncol. *34*, 2115–2124.

Arafeh, R., Qutob, N., Emmanuel, R., Keren-Paz, A., Madore, J., Elkahloun, A., Wilmott, J.S., Gartner, J.J., Di Pizio, A., Winograd-Katz, S., et al. (2015). Recurrent inactivating RASA2 mutations in melanoma. Nat. Genet. *47*, 1408–1410.

Bollag, G., Clapp, D.W., Shih, S., Adler, F., Zhang, Y.Y., Thompson, P., Lange, B.J., Freedman, M.H., McCormick, F., Jacks, T., and Shannon, K. (1996). Loss of NF1 results in activation of the Ras signaling pathway and leads to aberrant growth in haematopoietic cells. Nat. Genet. *12*, 144–148.

Bose, R., Kavuri, S.M., Searleman, A.C., Shen, W., Shen, D., Koboldt, D.C., Monsey, J., Goel, N., Aronson, A.B., Li, S., et al. (2013). Activating HER2 mutations in HER2 gene amplification negative breast cancer. Cancer Discov. *3*, 224–237.

Burke, J.E., Perisic, O., Masson, G.R., Vadas, O., and Williams, R.L. (2012). Oncogenic mutations mimic and enhance dynamic events in the natural activation of phosphoinositide 3-kinase p110alpha (PIK3CA). Proc. Natl. Acad. Sci. U S A *109*, 15259–15264.

Camidge, D.R., Pao, W., and Sequist, L.V. (2014). Acquired resistance to TKIs in solid tumours: learning from lung cancer. Nat. Rev. Clin. Oncol. *11*, 473–481.

Castellano, E., and Downward, J. (2011). RAS interaction with PI3K: more than just another effector pathway. Genes Cancer *2*, 261–274.

Chen, P.C., Yin, J., Yu, H.W., Yuan, T., Fernandez, M., Yung, C.K., Trinh, Q.M., Peltekova, V.D., Reid, J.G., Tworog-Dube, E., et al. (2014). Next-generation sequencing identifies rare variants associated with Noonan syndrome. Proc. Natl. Acad. Sci. U S A *111*, 11473–11478.

Cheung, L.W., and Mills, G.B. (2016). Targeting therapeutic liabilities engendered by PIK3R1 mutations for cancer treatment. Pharmacogenomics *17*, 297–307.

Chou, T.C. (2010). Drug combination studies and their synergy quantification using the Chou-Talalay method. Cancer Res. *70*, 440–446.

Cibulskis, K., Lawrence, M.S., Carter, S.L., Sivachenko, A., Jaffe, D., Sougnez, C., Gabriel, S., Meyerson, M., Lander, E.S., and Getz, G. (2013). Sensitive detection of somatic point mutations in impure and heterogeneous cancer samples. Nat. Biotechnol. *31*, 213–219.

Cocco, E., Javier Carmona, F., Razavi, P., Won, H.H., Cai, Y., Rossi, V., Chan, C., Cownie, J., Soong, J., Toska, E., et al. (2018). Neratinib is effective in breast tumors bearing both amplification and mutation of ERBB2 (HER2). Sci. Signal. *11*, https://doi.org/10.1126/scisignal.aat9773.

Corcoran, R.B., Rothenberg, S.M., Hata, A.N., Faber, A.C., Piris, A., Nazarian, R.M., Brown, R.D., Godfrey, J.T., Winokur, D., Walsh, J., et al. (2013). TORC1 suppression predicts responsiveness to RAF and MEK inhibition in BRAF-mutant melanoma. Sci. Transl. Med. *5*, 196ra198.

Croessmann, S., Sheehan, J.H., Lee, K.M., Sliwoski, G., He, J., Nagy, R., Riddle, D., Mayer, I.A., Balko, J.M., Lanman, R., et al. (2018). PIK3CA C2 domain deletions hyperactivate phosphoinositide 3-kinase (PI3K), generate oncogene dependence, and are exquisitely sensitive to PI3Kalpha inhibitors. Clin. Cancer Res. *24*, 1426–1435.

Croessmann, S., Formisano, L., Kinch, L.N., Gonzalez-Ericsson, P.I., Sudhan, D.R., Nagy, R.J., Mathew, A., Bernicker, E.H., Cristofanilli, M., He, J., et al. (2019). Combined blockade of activating ERBB2 mutations and ER results in synthetic lethality of ER+/HER2 mutant breast cancer. Clin. Cancer Res. *25*, 277–289.

Dasgupta, B., Yi, Y., Chen, D.Y., Weber, J.D., and Gutmann, D.H. (2005). Proteomic analysis reveals hyperactivation of the mammalian target of rapamycin pathway in neurofibromatosis 1-associated human and mouse brain tumors. Cancer Res. *65*, 2755–2760.

DeRose, Y.S., Wang, G., Lin, Y.C., Bernard, P.S., Buys, S.S., Ebbert, M.T., Factor, R., Matsen, C., Milash, B.A., Nelson, E., et al. (2011). Tumor grafts derived from women with breast cancer authentically reflect tumor pathology, growth, metastasis and disease outcomes. Nat. Med. *17*, 1514–1520.

Eichhorn, P.J., Gili, M., Scaltriti, M., Serra, V., Guzman, M., Nijkamp, W., Beijersbergen, R.L., Valero, V., Seoane, J., Bernards, R., and Baselga, J. (2008). Phosphatidylinositol 3-kinase hyperactivation results in lapatinib resistance that is reversed by the mTOR/phosphatidylinositol 3-kinase inhibitor NVP-BEZ235. Cancer Res. *68*, 9221–9230.

Faber, A.C., Coffee, E.M., Costa, C., Dastur, A., Ebi, H., Hata, A.N., Yeo, A.T., Edelman, E.J., Song, Y., Tam, A.T., et al. (2014). mTOR inhibition specifically sensitizes colorectal cancers with KRAS or BRAF mutations to BCL-2/BCL-XL inhibition by suppressing MCL-1. Cancer Discov. *4*, 42–52.

Frampton, G.M., Fichtenholtz, A., Otto, G.A., Wang, K., Downing, S.R., He, J., Schnall-Levin, M., White, J., Sanford, E.M., An, P., et al. (2013). Development and validation of a clinical cancer genomic profiling test based on massively parallel DNA sequencing. Nat. Biotechnol. *31*, 1023–1031.

Furet, P., Guagnano, V., Fairhurst, R.A., Imbach-Weese, P., Bruce, I., Knapp, M., Fritsch, C., Blasco, F., Blanz, J., Aichholz, R., et al. (2013). Discovery of NVP-BYL719 a potent and selective phosphatidylinositol-3 kinase alpha inhibitor selected for clinical evaluation. Bioorg. Med. Chem. Lett. *23*, 3741–3748.

Gandhi, L., Besse, B., Mazieres, J., Waqar, S., Cortot, A., Barlesi, F., Quoix, E., Otterson, G., Ettinger, D., Horn, L., and Moro-Sibilot, D. (2016). Neratinib ± temsirolimus in HER2-mutant lung cancers: an international, randomized phase II study. J. Thorac. Oncol. *12*, S358–S359.

Garcia-Garcia, C., Ibrahim, Y.H., Serra, V., Calvo, M.T., Guzman, M., Grueso, J., Aura, C., Perez, J., Jessen, K., Liu, Y., et al. (2012). Dual mTORC1/2 and HER2 blockade results in antitumor activity in preclinical models of breast cancer resistant to anti-HER2 therapy. Clin. Cancer Res. *18*, 2603–2612.

Guo, Y., Zhao, S., Ye, F., Sheng, Q., and Shyr, Y. (2014). MultiRankSeq: multiperspective approach for RNAseq differential expression analysis and quality control. Biomed. Res. Int. *2014*, 248090.

Gupta, S., Ramjaun, A.R., Haiko, P., Wang, Y., Warne, P.H., Nicke, B., Nye, E., Stamp, G., Alitalo, K., and Downward, J. (2007). Binding of ras to phosphoinositide 3-kinase p110alpha is required for ras-driven tumorigenesis in mice. Cell *129*, 957–968.

Halaban, R., and Krauthammer, M. (2016). RASopathy gene mutations in melanoma. J. Invest. Dermatol. *136*, 1755–1759.

Han, J., Flemington, C., Houghton, A.B., Gu, Z., Zambetti, G.P., Lutz, R.J., Zhu, L., and Chittenden, T. (2001). Expression of bbc3, a pro-apoptotic BH3-only gene, is regulated by diverse cell death and survival signals. Proc. Natl. Acad. Sci. U S A *98*, 11318–11323.

Hanker, A.B., Brewer, M.R., Sheehan, J.H., Koch, J.P., Sliwoski, G.R., Nagy, R., Lanman, R., Berger, M.F., Hyman, D.M., Solit, D.B., et al. (2017). An acquired HER2(T798I) gatekeeper mutation induces resistance to neratinib in a patient with HER2 mutant-driven breast cancer. Cancer Discov. *7*, 575–585.

Hay, N., and Sonenberg, N. (2004). Upstream and downstream of mTOR. Genes Dev. *18*, 1926–1945.

Huang, C.H., Mandelker, D., Schmidt-Kittler, O., Samuels, Y., Velculescu, V.E., Kinzler, K.W., Vogelstein, B., Gabelli, S.B., and Amzel, L.M. (2007). The structure of a human p110alpha/p85alpha complex elucidates the effects of oncogenic PI3Kalpha mutations. Science *318*, 1744–1748.

Hyman, D.M., Piha-Paul, S.A., Won, H., Rodon, J., Saura, C., Shapiro, G.I., Juric, D., Quinn, D.I., Moreno, V., Doger, B., et al. (2018). HER kinase inhibition in patients with HER2- and HER3-mutant cancers. Nature *554*, 189–194.

Jaiswal, B.S., Janakiraman, V., Kljavin, N.M., Chaudhuri, S., Stern, H.M., Wang, W., Kan, Z., Dbouk, H.A., Peters, B.A., Waring, P., et al. (2009). Somatic mutations in p85alpha promote tumorigenesis through class IA PI3K activation. Cancer Cell *16*, 463–474.

James, M.F., Han, S., Polizzano, C., Plotkin, S.R., Manning, B.D., Stemmer-Rachamimov, A.O., Gusella, J.F., and Ramesh, V. (2009). NF2/merlin is a novel negative regulator of mTOR complex 1, and activation of mTORC1 is associated with meningioma and schwannoma growth. Mol. Cell. Biol. *29*, 4250–4261.

Johannessen, C.M., Reczek, E.E., James, M.F., Brems, H., Legius, E., and Cichowski, K. (2005). The NF1 tumor suppressor critically regulates TSC2 and mTOR. Proc. Natl. Acad. Sci. U S A *102*, 8573–8578.

Kavuri, S.M., Jain, N., Galimi, F., Cottino, F., Leto, S.M., Migliardi, G., Searleman, A.C., Shen, W., Monsey, J., Trusolino, L., et al. (2015). HER2 activating mutations are targets for colorectal cancer treatment. Cancer Discov. *5*, 832–841.

Lai, W.V., Lebas, L., Barnes, T.A., Milia, J., Ni, A., Gautschi, O., Peters, S., Ferrara, R., Plodkowski, A.J., Kavanagh, J., et al. (2019). Afatinib in patients with metastatic or recurrent HER2-mutant lung cancers: a retrospective international multicentre study. Eur. J. Cancer *109*, 28–35.

Lanman, R.B., Mortimer, S.A., Zill, O.A., Sebisanovic, D., Lopez, R., Blau, S., Collisson, E.A., Divers, S.G., Hoon, D.S., Kopetz, E.S., et al. (2015).

Analytical and clinical validation of a digital sequencing panel for quantitative, highly accurate evaluation of cell-free circulating tumor DNA. PLoS One 10, e0140712.

Laplante, M., and Sabatini, D.M. (2009). mTOR signaling at a glance. J. Cell Sci. 122, 3589–3594.

Li, H., and Durbin, R. (2010). Fast and accurate long-read alignment with Burrows-Wheeler transform. Bioinformatics 26, 589–595.

Li, B.T., Shen, R., Buonocore, D., Olah, Z.T., Ni, A., Ginsberg, M.S., Ulaner, G.A., Offin, M., Feldman, D., Hembrough, T., et al. (2018). Ado-trastuzumab emtansine for patients with HER2-mutant lung cancers: results from a phase II basket trial. J. Clin. Oncol. 36, 2532–2537.

Ma, C.X., Bose, R., Gao, F., Freedman, R.A., Telli, M.L., Kimmick, G., Winer, E., Naughton, M., Goetz, M.P., Russell, C., et al. (2017). Neratinib efficacy and circulating tumor DNA detection of HER2 mutations in HER2 nonamplified metastatic breast cancer. Clin. Cancer Res. 23, 5687–5695.

Magnuson, B., Ekim, B., and Fingar, D.C. (2012). Regulation and function of ribosomal protein S6 kinase (S6K) within mTOR signalling networks. Biochem. J. 441, 1–21.

Mandelker, D., Gabelli, S.B., Schmidt-Kittler, O., Zhu, J., Cheong, I., Huang, C.H., Kinzler, K.W., Vogelstein, B., and Amzel, L.M. (2009). A frequent kinase domain mutation that changes the interaction between PI3Kalpha and the membrane. Proc. Natl. Acad. Sci. U S A 106, 16996–17001.

Miled, N., Yan, Y., Hon, W.C., Perisic, O., Zvelebil, M., Inbar, Y., Schneidman-Duhovny, D., Wolfson, H.J., Backer, J.M., and Williams, R.L. (2007). Mechanism of two classes of cancer mutations in the phosphoinositide 3-kinase catalytic subunit. Science 317, 239–242.

Miller, M.S., Schmidt-Kittler, O., Bolduc, D.M., Brower, E.T., Chaves-Moreira, D., Allaire, M., Kinzler, K.W., Jennings, I.G., Thompson, P.E., Cole, P.A., et al. (2014). Structural basis of nSH2 regulation and lipid binding in PI3Kalpha. Oncotarget 5, 5198–5208.

Nayar, U., Cohen, O., Kapstad, C., Cuoco, M.S., Waks, A.G., Wander, S.A., Painter, C., Freeman, S., Persky, N.S., Marini, L., et al. (2019). Acquired HER2 mutations in ER(+) metastatic breast cancer confer resistance to estrogen receptor-directed therapies. Nat. Genet. 51, 207–216.

O'Brien, N.A., McDonald, K., Tong, L., von Euw, E., Kalous, O., Conklin, D., Hurvitz, S.A., di Tomaso, E., Schnell, C., Linnartz, R., et al. (2014). Targeting PI3K/mTOR overcomes resistance to HER2-targeted therapy independent of feedback activation of AKT. Clin. Cancer Res. 20, 3507–3520.

Perera, S.A., Li, D., Shimamura, T., Raso, M.G., Ji, H., Chen, L., Borgman, C.L., Zaghlul, S., Brandstetter, K.A., Kubo, S., et al. (2009). HER2YVMA drives rapid development of adenosquamous lung tumors in mice that are sensitive to BIBW2992 and rapamycin combination therapy. Proc. Natl. Acad. Sci. U S A 106, 474–479.

Pirazzoli, V., Nebhan, C., Song, X., Wurtz, A., Walther, Z., Cai, G., Zhao, Z., Jia, P., de Stanchina, E., Shapiro, E.M., et al. (2014). Acquired resistance of EGFR-mutant lung adenocarcinomas to afatinib plus cetuximab is associated with activation of mTORC1. Cell Rep. 7, 999–1008.

Prabowo, A.S., Iyer, A.M., Veersema, T.J., Anink, J.J., Schouten-van Meeteren, A.Y., Spliet, W.G., van Rijen, P.C., Ferrier, C.H., et al. (2014). BRAF V600E mutation is associated with mTOR signaling activation in glioneuronal tumors. Brain Pathol. 24, 52–66.

Razavi, P., Chang, M.T., Xu, G., Bandlamudi, C., Ross, D.S., Vasan, N., Cai, Y., Bielski, C.M., Donoghue, M.T.A., Jonsson, P., et al. (2018). The genomic landscape of endocrine-resistant advanced breast cancers. Cancer Cell 34, 427–438.e6.

Robichaux, J.P., Elamin, Y.Y., Tan, Z., Carter, B.W., Zhang, S., Liu, S., Li, S., Chen, T., Poteete, A., Estrada-Bernal, A., et al. (2018). Mechanisms and clinical

activity of an EGFR and HER2 exon 20-selective kinase inhibitor in non-small cell lung cancer. Nat. Med. 24, 638–646.

Rodriguez-Viciana, P., Warne, P.H., Dhand, R., Vanhaesebroeck, B., Gout, I., Fry, M.J., Waterfield, M.D., and Downward, J. (1994). Phosphatidylinositol-3-OH kinase as a direct target of Ras. Nature 370, 527–532.

Shaw, R.J., and Cantley, L.C. (2006). Ras, PI(3)K and mTOR signalling controls tumour cell growth. Nature 441, 424–430.

Sheng, Q., Vickers, K., Zhao, S., Wang, J., Samuels, D.C., Koues, O., Shyr, Y., and Guo, Y. (2017). Multi-perspective quality control of Illumina RNA sequencing data analysis. Brief Funct. Genomics 16, 194–204.

Shihab, H.A., Rogers, M.F., Gough, J., Mort, M., Cooper, D.N., Day, I.N., Gaunt, T.R., and Campbell, C. (2015). An integrative approach to predicting the functional effects of non-coding and coding sequence variation. Bioinformatics 31, 1536–1543.

Shimamura, T., Ji, H., Minami, Y., Thomas, R.K., Lowell, A.M., Shah, K., Greulich, H., Glatt, K.A., Meyerson, M., Shapiro, G.I., and Wong, K.K. (2006). Non-small-cell lung cancer and Ba/F3 transformed cells harboring the ERBB2 G776insV_G/C mutation are sensitive to the dual-specific epidermal growth factor receptor and ERBB2 inhibitor HKI-272. Cancer Res. 66, 6487–6491.

Solit, D.B., Garraway, L.A., Pratilas, C.A., Sawai, A., Getz, G., Basso, A., Ye, Q., Lobo, J.M., She, Y., Osman, I., et al. (2006). BRAF mutation predicts sensitivity to MEK inhibition. Nature 439, 358–362.

Subramanian, A., Narayan, R., Corsello, S.M., Peck, D.D., Natoli, T.E., Lu, X., Gould, J., Davis, J.F., Tubelli, A.A., Asiedu, J.K., et al. (2017). A next generation connectivity map: L1000 platform and the first 1,000,000 profiles. Cell 171, 1437–1452.e17.

Sun, M., Hillmann, P., Hofmann, B.T., Hart, J.R., and Vogt, P.K. (2010). Cancer-derived mutations in the regulatory subunit p85alpha of phosphoinositide 3-kinase function through the catalytic subunit p110alpha. Proc. Natl. Acad. Sci. U S A 107, 15547–15552.

Teh, J.L.F., Cheng, P.F., Purwin, T.J., Nikbakht, N., Patel, P., Chervoneva, I., Ertel, A., Fortina, P.M., Kleiber, I., HooKim, K., et al. (2018). In vivo E2F reporting reveals efficacious schedules of MEK1/2-CDK4/6 targeting and mTOR-S6 resistance mechanisms. Cancer Discov. 8, 568–581.

Wong, K.K., Fracasso, P.M., Bukowski, R.M., Lynch, T.J., Munster, P.N., Shapiro, G.I., Janne, P.A., Eder, J.P., Naughton, M.J., Ellis, M.J., et al. (2009). A phase I study with neratinib (HKI-272), an irreversible pan ErbB receptor tyrosine kinase inhibitor, in patients with solid tumors. Clin. Cancer Res. 15, 2552–2558.

Wu, H., Shekar, S.C., Flinn, R.J., El-Sibai, M., Jaiswal, B.S., Sen, K.I., Janakiraman, V., Seshagiri, S., Gerfen, G.J., Girvin, M.E., and Backer, J.M. (2009). Regulation of Class IA PI 3-kinases: C2 domain-iSH2 domain contacts inhibit p85/p110alpha and are disrupted in oncogenic p85 mutants. Proc. Natl. Acad. Sci. U S A 106, 20258–20263.

Yang, H., and Wang, K. (2015). Genomic variant annotation and prioritization with ANNOVAR and wANNOVAR. Nat. Protoc. 10, 1556–1566.

Yu, H.A., Suzawa, K., Jordan, E., Zehir, A., Ni, A., Kim, R., Kris, M.G., Hellmann, M.D., Li, B.T., Somwar, R., et al. (2018). Concurrent alterations in EGFR-mutant lung cancers associated with resistance to EGFR kinase inhibitors and characterization of MTOR as a mediator of resistance. Clin. Cancer Res. 24, 3108–3118.

Zabransky, D.J., Yankaskas, C.L., Cochran, R.L., Wong, H.Y., Croessmann, S., Chu, D., Kavuri, S.M., Red Brewer, M., Rosen, D.M., Dalton, W.B., et al. (2015). HER2 missense mutations have distinct effects on oncogenic signaling and migration. Proc. Natl. Acad. Sci. U S A 112, E6205–E6214.

STAR★METHODS

KEY RESOURCES TABLE

REAGENT or RESOURCE	SOURCE	IDENTIFIER
Antibodies		
pHER2 (Y1248)	Cell Signaling Technologies	Cat# 2244; RRID: AB_331705
HER2	Cell Signaling Technologies	Cat# 2242; RRID: AB_331015
pAKT (S473)	Cell Signaling Technologies	Cat# 9271; RRID: AB_329825
pAKT (T308)	Cell Signaling Technologies	Cat# 13038; RRID: AB_2629447
pERK	Cell Signaling Technologies	Cat# 9101S; RRID: AB_331646
pS6 (240/4)	Cell Signaling Technologies	Cat# 2215S; RRID: AB_331682
pS6 (235/6)	Cell Signaling Technologies	Cat# 2211S; RRID: AB_331679
pS6K (T389)	Cell Signaling Technologies	Cat# 9205; RRID: AB_330944
pmTOR (S2448)	Cell Signaling Technologies	Cat# 2971S; RRID: AB_330970
Bacterial and Virus Strains		
One Shot™ MAX Efficiency™ DH5α™-T1	Thermo Fisher Scientific	Cat# 12297016
One Shot™ Stbl3™ Chemically Competent cells	Thermo Fisher Scientific	Cat# C737303
Biological Samples		
ST1616B (*HER2*-amplified, *HER2*^{D769Y}) breast PDX	START	N/A
ST1456 (*HER2*^{V842I}) breast PDX	START	N/A
HCI003 (*HER2* $^{G778\_P780\ dup}$) breast PDX	Gift from Dr. Alan Welm, Huntsman Cancer Institute	N/A
Chemicals		
Neratinib (HKI-272)	PUMA biotechnology / Selleck Chemicals	Cat# S2150
Everolimus (RAD001)	Selleck Chemicals	Cat# S1120
Alpelisib (BYL719)	Novartis	N/A
Buparlisib (BKM120)	Selleck Chemicals	Cat# S2247
MK2206	Selleck Chemicals	Cat# S1078
Afatinib (BIBW2992)	Selleck Chemicals	Cat# S7810
Lapatinib	LC laboratories	N/A
Selumetinib (AZD6244)	Selleck Chemicals	Cat# S1008
Critical Commercial Assays		
Ras Activation Assay Kit	EMD Millipore	Cat# 17-218
Deposited Data		
RNA-sequencing	GEO database	Accession ID: GSE128730
Whole exome sequencing	SRA database	BioProject ID: PRJNA574429
Experimental Models: Cell Lines		
5637 *HER2*^{S310F} cell line	ATCC	Cat# HTB-9
H1781 *HER2* $^{G776>VC}$ cell line	ATCC	Cat# CRL-5894
OVCAR8 *HER2*^{G776V} cell line	DCDT tumor repository,NCI	N/A
MCF7 *HER2*^{V777L} cell line	Gift from Dr. Ben Park, Vanderbilt Ingram Cancer Center	N/A
MCF7 *HER2*^{L755S} cell line	Gift from Dr. Ben Park, Vanderbilt Ingram Cancer Center	N/A
DV90 *HER2*^{V842I} cell line	DSMZ	Cat# ACC 307
SNUC2A *HER2*^{R678Q} cell line	ATCC	Cat# CCL-250.1
Oligonucleotides		
Silencer® Select RPTOR siRNA	Thermo Fisher Scientific	Assay ID s33216
Silencer® Select RPTOR siRNA	Thermo Fisher Scientific	Assay ID s33215

Continued

REAGENT or RESOURCE	SOURCE	IDENTIFIER
Silencer® Select RHEB siRNA	Thermo Fisher Scientific	Assay ID s12019
Silencer® Select HRAS siRNA (validated)	Thermo Fisher Scientific	Assay ID: 120898
Silencer® Select KRAS siRNA (validated)	Thermo Fisher Scientific	Assay ID 120703
Silencer® Select NRAS siRNA (validated)	Thermo Fisher Scientific	Assay ID: 120250
Recombinant DNA		
pLKO.1-TSC2 (shRNA)	Addgene	Cat# 15478
NF1 (Myc-DDK-tagged)-Human neurofibromin 1 (NF1), transcript variant 1	OriGene Technologies	Cat# RC220425
pDONR223_PIK3CA_WT	Addgene	Cat# 81736
pDONR223_PIK3CA_p.H1047R	Addgene	Cat# 82824
pDONR223_KRAS_WT	Addgene	Cat# 81923
pDONR223_KRAS_GV12	Addgene	Cat# 31200
Lenti-ORF clone of RASA2 (Myc-DDK-tagged)-Human RAS p21 protein activator 2 (RASA2)	OriGene Technologies	Cat# RC224076L3
Software and Algorithms		
Compusyn software	PMID:20068163	N/A

LEAD CONTACT AND MATERIAL AVAILABILITY

Requests for plasmids, resistant cell lines, and other reagents generated in this study should be directed to and will be fulfilled by the lead contact, Dr. Carlos Arteaga at carlos.arteaga@utsouthwestern.edu. There are restrictions to the availability of neratinib-resistant PDXs due to a Material Transfer Agreement with START.

EXPERIMENTAL MODELS AND SUBJECT DETAILS

Cell Lines

5637 ($ERBB2^{S310F}$, bladder cancer; ATCC® HTB-9™), OVCAR8 ($ERBB2^{G776V}$, ovarian cancer; purchased from DCDT tumor repository, NCI), H1781 ($ERBB2^{G776>VC}$, lung cancer; ATCC® CRL-5894™), DV90 ($ERBB2^{V842I}$, lung cancer; DSMZ® ACC 307) and SNUC2A ($ERBB2^{R678Q}$, colorectal cancer; ATCC® CCL-250.1™) cell lines were maintained in recommended media supplemented with 10% FBS (Gibco) at 37°C in a humidified atmosphere of 5% CO_2 in air. HER2 copy number and immunohistochemical analysis were performed on 5637 and OVCAR8 cells (Figures S1A–S1C). Breast cancer MCF7 cells with knock-in L755S and V777L $HER2$-activating mutations were gifts from Dr. Ben Park. All cell lines were tested for mycoplasma contamination and authenticated by short tandem repeat (STR) profiling in January 2019. Drug-resistant cells were developed by exposing cells to increasing concentrations of neratinib over 6-8 months (5637^{NR}, 600 nM; $OVCAR8^{NR}$, 1 μM). Prior to performing any experiment with neratinib-resistant cells, cells were maintained under drug-free conditions for 72-96 hr. Experiments with $MCF7^{L755S}$ and $MCF7^{V777L}$ cells were performed in estrogen-free media supplemented with 10% charcoal stripped serum.

Mouse Models

All animal experiments were approved by the Vanderbilt or UTSW Institutional Animal Care and Use Committee (IACUC protocols M/14/032 and 2018-102535). The ST1456 (ER-/PR-/$HER2^{V842I}$) and ST1616B (ER-/$HER2$-amplified; $HER2^{D769Y}$) (Cocco et al., 2018) PDXs were from START (San Antonio, Texas). HCI-003 PDXs (ER+/$HER2^{G778\_P780dup}$) were obtained from Alana Welm (DeRose et al., 2011).

Patient Studies

The SUMMIT trial (NCT01953926) was conducted in accordance with the Declaration of Helsinki and approved by the institutional review boards of all participating institutions (Hyman et al., 2018). Written informed consent was obtained from all patients described in the study. Tissue based targeted capture next-generation DNA sequencing was performed by Foundation medicine using the FoundationOne™ panel as described previously (Frampton et al., 2013). Plasma cfDNA sequencing was performed by Guardant Health using the Guardant360 assay (Lanman et al., 2015).

METHOD DETAILS

Cell Viability Assays

For dose-response assays, parental and neratinib-resistant cells were seeded in 12-well plates; 24 hr later, cells were treated with DMSO or increasing concentrations of neratinib (11 doses ranging from 0.1 nM to 10 μM, 3-fold dilution). Six days later, cells were trypsinized and counted using Z2 particle count analyzer (Beckman Coulter). GraphPad Prism 6 software was used to plot dose response curves and determine GI_{50} concentration.

RNA Sequencing and cDNA Library Construction

5637^{NR} and $OVCAR8^{NR}$ cells were maintained under drug-free conditions for 1 week prior to seeding. Parental and neratinib-resistant cells were seeded in triplicate in 10-cm dishes and then treated with or without neratinib (5637 – 600 nM; OVCAR8 – 1 μM); 24 hr later, cells were harvested and RNA was purified using ReliaPrep RNA Cell Miniprep system (Promega). Total RNA was quantified using the Quant-iT Ribo-Green RNA Assay Kit (Invitrogen). Automated Illumina Tru Seq Sample Preparation protocol was used to separate mRNA from total RNA, followed by cDNA synthesis. Libraries were prepared using TruSeq® Stranded mRNA Library Prep kit (Illumina). Following quality check, the libraries were quantified using the KAPA Library Quantification Kits for Next-Generation Sequencing (Kapa biosystems), pooled and sequenced on the HiSEq3000 platform targeting 50 million paired end reads/sample.

RNAseq data were thoroughly quality controlled at multiple stages of data processing as described earlier (Sheng et al., 2017). Raw data and alignment QC were performed using QC3 software. Raw data were aligned with TopHat 2 against Human GRCh38 reference genome and read count data were obtained using HTSeq. Differential gene expression analysis were carried out using DESeq (Guo et al., 2014). False discovery rate (FDR) <0.05 was used to correct for multiple testing. Functional analyses were performed using Gene Set Enrichment Analysis (GSEA).

Whole Exome Sequencing

Parental and neratinib-resistant cells were seeded in 10-cm dishes. 24 hr later, cells were harvested and DNA was purified using Maxwell 16 DNA purification kit (Promega). Genomic DNA was quantified using the Quant-iT Pico-Green DNA Assay Kit (Invitrogen). Library preparation and capture was completed using the Agilent Whole Exome protocol. Following quality control assay, libraries were quantified using the KAPA Library Quantification Kits for Next-Generation Sequencing (Kapa biosystems). Samples were normalized, pooled, and sequenced on the HiSeq3000 platform targeting 20 million paired end reads/sample. Whole exome reads were aligned to the human reference genome hg19 using BWA (Li and Durbin, 2010), sorted and indexed by Samtools. Duplicates reads were marked and base quality scores were recalibrated. Mutect (Cibulskis et al., 2013) was used to detect mutations that are acquired in resistance cell lines but not present in matched sensitive cells. The functional effects of variants were annotated by ANNOVAR (Yang and Wang, 2015).

Immunoblot Analysis

Cells were washed with ice-cold PBS and lysed with RIPA buffer (Sigma) supplemented with 1X protease inhibitor (Roche) and phosphatase inhibitor (Roche) cocktails. Snap-frozen tumor fragments were homogenized using the TissueLyser (Qiagen) and lysed in buffer containing 50 mM Tris-HCl pH 8.0, 150 mM NaCl, 2 mM EDTA pH 8.0, 10 mM NaF, 20% glycerol, 1% Nonidet P-40 plus protease and phosphatase inhibitors. Lysates were rocked on an orbital shaker at 4°C for 30 min followed by centrifugation at 13,500 rpm for 15 min. Protein concentrations in supernatants were quantified using BCA protein assay kit (Pierce). 40 μg of total protein were fractionated on bis-tris 4-12% gradient gels (NuPAGE) and transferred to nitrocellulose membranes (BioRad). Membranes were blocked with 5% non-fat dry milk at room-temperature for 1 hr, followed by overnight incubation with primary antibodies of interest at 4°C. All antibodies were purchased from Cell Signaling – P-HER2 Y1248 (#2244; 1:500), HER2 (#2242; 1:1000), P-EGFR Y1068 (#2234; 1:500); P-HER3 Y1197 (#4561; 1:500), P-mTOR S2448 (#2971; 1:500), m-TOR (#2983; 1:1000), P-AKT S473 (#9271; 1:500), P-S6 S235/6 (#2211; 1:1000), PS6 S240/4 (#2215; 1:1000), P-ERK T202/Y204 (#9101; 1:1000), P-S6 kinase T389 (#9208; 1:1000), P-4EBP-1 (#2855; 1:1000); β-actin (#4970; 1:3000). Nitrocellulose membranes were washed and incubated with HRP-conjugated α-rabbit or α-mouse secondary antibodies for 1-2 hr at room temperature. Protein bands were detected with an enhanced chemiluminescence substrate (Perkin Elmer).

siRNA Transfections

Silencer Select pre-designed siRNA targeting *RAPTOR*, *RHEB*, *RICTOR*, or *RAS*-isoforms were purchased from Ambion. Cells were reverse-transfected with siRNAs of interest using lipofectamine RNAiMAX transfection reagent (ThermoFisher Scientific) as per manufacturer's instructions; 48 hr post-transfection, cells were treated with indicated concentrations of neratinib.

Xenograft Studies

5637^{NR} and $OVCAR8^{NR}$ cells were re-suspended in serum-free RPMI and Matrigel (1:1 ratio) and injected subcutaneously into the right flank of 4-6 week old female athymic nu/nu mice. The ST1456 (ER-/PR-/$HER2^{V842I}$) and ST1616B (ER-/$HER2$-amplified; $HER2^{D769Y}$) (Cocco et al., 2018) PDXs were implanted subcutaneously in nude mice. NSG mice were implanted with a 21-day estrogen pellet the day before HCI-003 PDX (ER+/$HER2^{G778\_P780dup}$) implantation. Tumor chunks were orthotopically implanted into the mammary fat pad. 4 weeks after tumor transplantation, mice were given 8 ug/ml estradiol in their drinking water for a duration

of 2 ½ weeks. Estradiol water was removed before treatment initiation. When the average tumor volume reached ~200 mm^3, mice received daily doses of neratinib (40 mg/kg; orogastric gavage), everolimus (5 mg/kg; orogastric gavage) or the combination. In our previous studies, we have found neratinib to cause anorexia and moderate body weight loss. To avoid these toxicities, all mice were prophylactically supplemented with DietGel 76A (Clear H$_2$O) in addition to regular chow. Tumor diameters were measured using calipers and tumor volumes were calculated as: volume = width^2 x length/2. At completion of the experiment, tumors were harvested 2-4 hr of the last drug administration and fixed in 10% neutral buffered formalin; 24 hr later, tumors were dehydrated and paraffin embedded. Tumor sections (5 μm) were immunostained for P-S6 (#2211, Cell Signaling) and scored by expert pathologists (P.G.E. and M.H.R). Staining scores were determined using a semi-quantitative weighted histoscoring system (H-score) that takes both intensity and percentage positivity into account using the formula: 3*[% of 3+ cells] + 2*[% of 2+ cells] + 1*[% of 1+ cells]. P-S6 staining was cytoplasmic.

Neratinib-resistant ST1616B (*HER2*-amplified, *HER2*^{D769Y}) breast cancer PDXs were generated through prolonged treatment of initially neratinib-sensitive PDXs. All 12 ST1616B tumors regressed upon neratinib treatment; 4 sensitive, regressing tumors were harvested after 5-7 weeks of therapy. The remaining 8/12 mice remained on treatment for a total of 120 days after which the treatment was stopped. After this, mice were monitored for tumor recurrence. Treatment was resumed when tumors reached 200 mm^3 in volume; 5/6 recurrent tumors were refractory to neratinib retreatment of which 4 were harvested when they reached >450 mm^3 on continuous therapy.

Organoid Establishment and Culture

Fresh/frozen tumor chunks were rinsed twice with 10 ml AdDF+++ media (advanced DMEM/F12 containing 1X Glutamax, 10 mM HEPES and antibiotics) and minced into 1-2 mm pieces. 10 ml dissociation media (1:1 vol/vol F12, DMEM supplemented with 2% w/v bovine serum albumin, 300 U/ml collagenase, 100 U/ml hyaluronidase, 10 ng/ml epidermal growth factor (EGF), 1 mg/ml insulin, and 0.5 mg/ml hydrocortisone) was added to tumor fragments and incubated for 2 hr at 37°C with constant shaking at 275 rpm. Dissociated tumor fragments were centrifuged at 1200 rpm for 5 min and subjected to RBC lysis as per manufacturer's protocol (BD Biosciences), if the cell pellet was visibly red. Tumor fragments were further dissociated by adding 3 ml pre-warmed trypsin and incubating in a 37°C bead bath for 5-7 min. 6 ml neutralization solution (2% FBS in PBS) was added and centrifuged at 1200 rpm for 5 min. Tumor pellets were then treated with the Dispase/DNAse cocktail for 5-7 min at 37°C, and neutralized and centrifuged as above. If establishing organoids from PDXs, tumor cell suspension was subjected to magnetic separation of CD298+ human cells (α-CD298 antibody, MACs, #130107292) to eliminate potential mouse cell contamination, using EasySep human biotin positive selection kit II (STEMCELL technologies #17663). Cell pellet was resuspended in appropriate volume of cold BME and 40 μl of cell suspension was added to the center of each well of a 24-well plate and allowed to solidify by placing in a 37°C incubator for 20 min. 500 μl organoid medium was added to each well and the plate was returned to a 37°C incubator maintained at 2% O$_2$ level.

For viability assays, established organoids were dissociated into single cell suspension by mechanical shearing and enzymatic digestion using TrypLE express (Gibco, #12604021). 3000-10000 cells were resuspended in 100 μl of cold organoid media containing 5% BME and seeded into BME-coated 96-well plate. Once the organoids had established (approximately 3 days later), they were treated with drugs and the effect on viability was assessed 6 days later using CellTiter-Glo 3D viability assay kit (Promega # G9681).

Active RAS Pulldown Assay

5637^{NR} and OVCAR8^{NR} cells were grown in 150-mm dishes in the absence of neratinib for 72-96 hr. Parental and neratinib-resistant cells were then treated with indicated concentrations of neratinib for 6 hr. Cells were lysed with magnesium lysis buffer supplemented with aprotenin (10 μg/ml), Na$_3$VO$_4$ (1 mM) and pepstatin (10 μg/ml) and processed as per manufacturer's instructions (RAS activation assay kit, Millipore). Briefly, whole cell lysates were incubated with agarose beads bound to Ras Binding Domain (RBD) of Raf-1 protein for 45 min at 4°C. GTP-RAS bound agarose beads were centrifuged, washed thrice with magnesium lysis buffer, boiled in sample loading buffer and subjected to immunoblot analysis using a pan-RAS antibody (Millipore).

Analysis of Clinical de-novo Resistance to Neratinib

Baseline tumors from all patients enrolled in the phase II SUMMIT trial underwent targeted next generation DNA sequencing using the MSK-IMPACT panel (version 1 – 341 genes; version 2 – 410 genes). Tumor mutation profiles are available on SUMMIT, Nature 2018, http://www.cbioportal.org/study?id=summit_2018. Genes involved in RAS pathway and well-known activators of TORC1 in the PI3K pathway were considered as 'mTOR pathway activating alterations'. Even for these genes, only mutations that are classified as oncogenic by the OncoKB database were deemed mTOR pathway activators. Table S1 contains a list of genes that were considered 'mTOR pathway activating' and 'non-mTOR pathway' alterations. Mutations in RTKs other than HER2 and downstream members of the RAS pathway such as BRAF or MAPK were not considered to be mTOR activating in our analysis.

Structural Analysis of PIK3R1$^{558-561}$ Deletion

Structures corresponding to PIK3R1 were identified using the query sequence P27986.2 to search the PDB sequence database with BLAST. A number of identified structures correspond to various domains of PIK3R1, especially truncated constructs that include nSH2 and iSH2 (niSH2) that cover the PIK3R1 558-561 deletion and are bound to PIK3CA. To provide the structural context of the mutation, we selected crystal structures corresponding to PIK3CA in complex with niSH2 (residues 327-598) of PIK3R1 (PDB: 4ovu, 2.96 Å), the same complex bound to lipid diC4-PIP2 (PDB: 4ovv, 3.5 Å) (Miller et al., 2014), a better resolution structure of

the niSH2 complex bound to an inhibitor (PDB: 4jps, 2.2 Å) (Furet et al., 2013), and a structure of PIK3CA H1047R in complex with niSH2 of PIK3R1 and the drug wortmannin (PDB: 3hhm, 2.8 Å) (Mandelker et al., 2009). Since the interaction surface surrounding the deletion (defined by residues within 4 Å) is similar in all of the structures, we chose the wild type apo structure 4ovu for illustration.

QUANTIFICATION AND STATISTICAL ANALYSIS

Statistical Analysis

For analyses involving multiple comparisons, one-way ANOVA with Bonferroni post-hoc test was used. Student's t-test was used to analyze effect on cell proliferation, and *in vivo* tumor growth assays. Bar graphs show mean ± SEM, unless otherwise stated in the figure legend. GraphPad Prism software was used to plot dose response curves and determine IC_{50} concentration. For RNA sequencing, FDR <0.05 was used to correct for multiple testing.

DATA AND CODE AVAILABILITY

Data from cBioPortal and GENIE were downloaded from https://www.cbioportal.org/ and https://genie.cbioportal.org/, respectively. COSMIC mutation impact prediction tool and mutation database was accessed through https://cancer.sanger.ac.uk/cosmic. RNA sequencing data has been submitted to the GEO database (Accession ID: GSE128730). Whole exome sequencing data is available on the SRA database (BioProject ID: PRJNA574429).